POLITECNICO DI TORINO

Master's Degree in Aerospace Engineering

# Multiple Near Earth Asteroids rendezvous trajectories optimization with electric propulsion

Supervisor:
Prof. Lorenzo Casalino

Candidate:
Paolo Bossi

July 2019

*...a Mamma,*
*a Papà,*
*a Zia Lea...*

# Contents

# List of Figures

# List of Tables

# Abstract

Since ancient times, humankind has always been fascinated and intrigued by the sky and its celestial phenomena, always trying to understand the causes.

Over time this curiosity has led to the realization of the first space missions, revealing many secrets about our solar system. In the recent past, space agencies moved towards the exploration of our local neighborhood, studying the asteroids. They are indeed very useful to understand the history and formation of our solar system. But, unfortunately, today few missions have been planned: the most important were the Hayabusa 1 and 2 by JAXA, and OSIRIS-REx by NASA.

The growth of Near Earth Asteroids (NEA) discoveries, have increased the awareness and the probability of futures Earth impacts, causing the end of life on our planet. In recent years, numerous asteroids have been classified as potential hazards, and more informations are needed on their physical properties and their orbital parameters to better predict their future orbits.

Inaf NEST mission aims to analyze three NEA, with Apophis the main target, with a spacecraft equipped with electric propulsion. This technology make possible to have more flexibility in departure dates and a considerably reduction in fuel consumption. A multiple asteroid rendezvous with chemical propulsion is almost impossible, because there must be the correct angle phases between asteroids.

The following thesis aims to determine the possible asteroids to be reached and the optimal trajectories that reduce the fuel consumption, by using the Optimal Control Theory, respecting the NEST mission constraints:

- departure in 2028;
- duration less than five years;
- rendezvous with three Near Earth Asteroids,(one must be Apophis).

In particular, various departure date from the Earth have been selected over the year 2028 and different departure and arrive dates from the asteroids

have been selected, with multiple asteroids sequences. The best sequence was further analyzed, finding the best trajectories in terms of $\Delta V$ and duration.

# Chapter 1

# The Asteroids

## 1.1 The Main Asteroid Belt

Asteroids are small rocky celestial bodies rotating around the sun, typically between Mars and Jupiter with a semi-major axis $2.1 < a < 3.6$ AU, forming the Asteroids Main Belt. The first main belt object (Ceres) was discovered in 1801 by the italian astronomer Giuseppe Piazzi, and today more than one million asteroids are known, from the largest (with a diameter $D > 100km$) to the smallest (with a diameter $D < 0.1km$).

It is thought that the main belt originated during the solar system formation as a group of planetesimals, but because of Jupiter gravitational perturbations the planetesimals could not accrete and form a planet in that particular region, as expected by the Titius-Bode law. A confirmation of this theory arrives from the Kirkwood gaps, which are sudden decreases in the number of asteroids, in particular semi-major axes corresponding to the locations of orbital resonances with Jupiter. In figure 1.1 is possible to see the Kirkwood gaps in relation with semi-major axis.

Having formed at the beginning of the solar system, asteroids can be very useful for scientific research, they have in fact different elements, minerals, and chemical properties useful to understand the formation and the past of the solar system. They can be divided in three types:

- **C-Type** = mainly made of carbon, these are the most common asteroids in the main belt (75 %). They have a low albedo (because of carbon composition) and they are predominantly in the outer edge of the asteroid belt, 3.5 AU. They are very close in chemical composition to the primitive solar nebula;

- **M-Type** = mainly made of nickel and iron, these are the 10% of asteroid main belt. They are moderately bright (0.1-0.2 albedo);

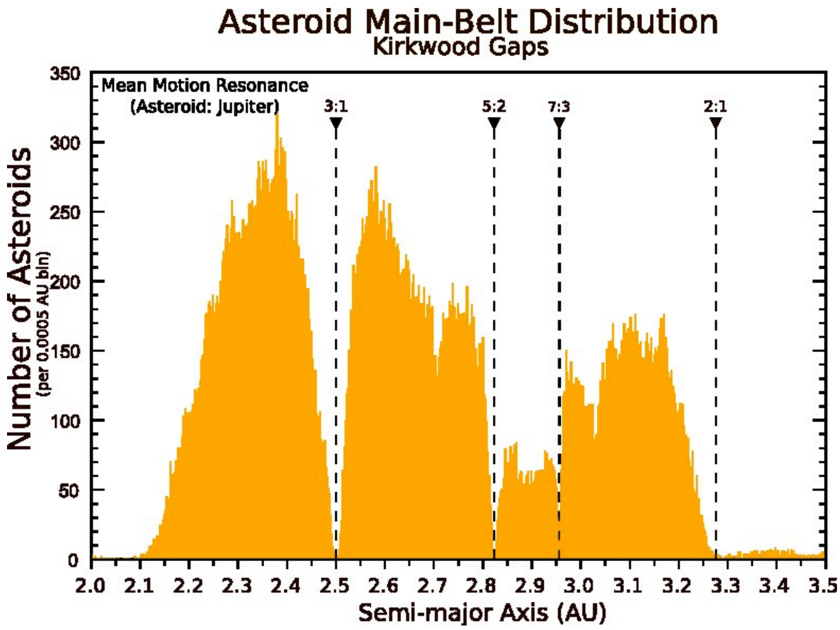


Figure 1.1: Asteroids main belt number respect to semi-major axis and Jupiter resonance [16]

- **S-Type** = mainly made of iron and magnesium silicates,these are approximately 17% of asteroids. They are moderately bright (0.2 albedo) and they are dominant in the inner part of the asteroid belt (2.2 AU) and common in the central part (3.0 AU).

## 1.2 Near Earth Asteroid

Because of Jupiter perturbations, some asteroids can escape from the main belt, reaching near Earth orbits. These asteroids are classified as near Earth object (NEO) and they must have a perihelion $p_r < 1.3$ AU . More than 20.000 objects are classified as NEO and can be summarized in figure 1.2 These asteroids can survive in their orbits for a short period ( 10/100 millions of years) : they can impact an inner planet or being perturbed ( flyby for example). To compensate the elimination of these bodies over time, there is a supply of asteroids from the main belt caused by Jupiter perturbations. NEO Asteroids are classified in four types based on their semi-major axis $a$, perihelion $r_p$ distance and aphelion distance $r_a$:

- **Atiras Asteroids**: these asteroids have the entire orbit inside Earth's orbit, in fact Atira asteroid's aphelion distance is smaller than Earth's perihelion;

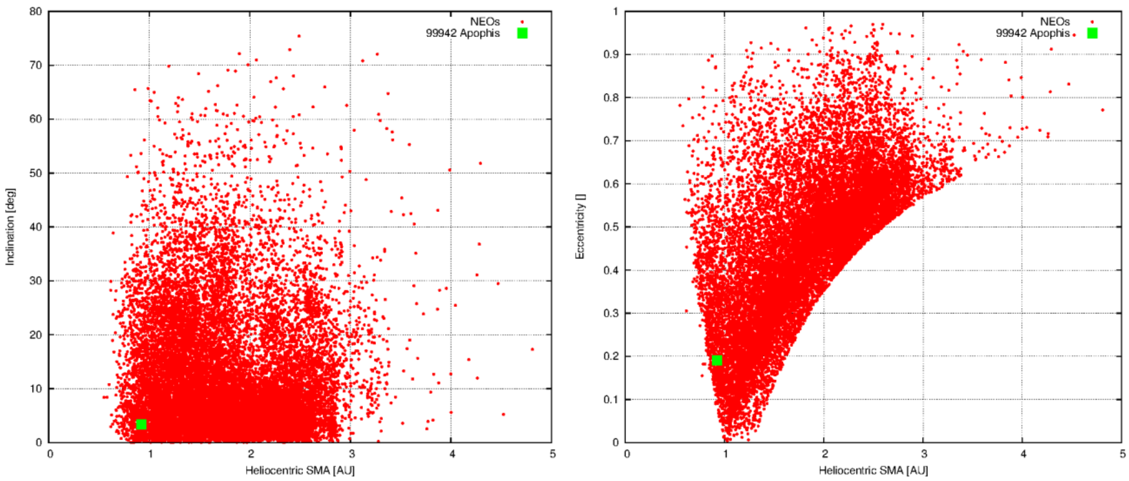


(a) (b)

Figure 1.2: Distribution of NEOs over semi-major axis, inclination (a), eccentricity (b).[17]

- **Athens Asteroids**: have a semi-major axis less than 1 AU, the aphelion distance is greater than Earth's perihelion.
- **Apollos Asteroids**: have a semi-major axis greater than 1 AU, the perihelion distance is smaller than Earth's aphelion;
- **Amors Asteroids**: have the entire orbit outside Earth's orbit; the perihelion distance is greater than Earth's aphelion.

As we can see in figure 1.3 the most dangerous asteroids families are Athens and Apollos, they intersect Earth's orbit, causing a possible risk of impact with the Earth. It is therefore necessary to survey constantly these asteroids, computing their future orbits and looking for future possible impacts.

To evaluate a NEO impact risk, in 1999 was created a risk scale, named Torino scale, which combines in a single value the impact probability with the potential damage of a NEO object; this scale is intended for public to assess the seriousness of collision predictions and take action with an adequate defense. The scale takes the name from the city where the conference took place in 1999 (Turin, Italy), it has a range between 0 a 10, where 0 indicates no impact risk with the Earth or the object is too small to penetrate Earth's atmosphere intact, while 10 indicates that a collision with the Earth is certain, causing a global disaster. A NEO object can be upgraded

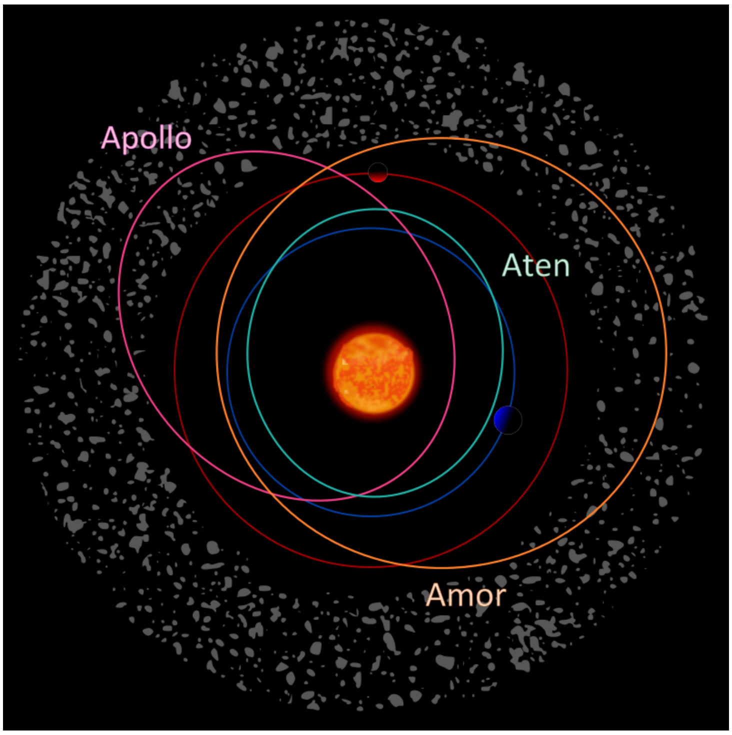


Figure 1.3: Near Earth Asteroid orbit types. [18]

or downgraded in the Torino scale with more observations and updated trajectories over time, and can have multiple potential collisions with multiple and different risk values. In figure 1.4 is possible to see the Torino scale.

The astronomers use another risk scale, the Palermo scale, which again combines the potential impact and the potential kinetic energy released in the impact in a logarithmic scale. The Palermo scale value is defined by the equation:

$$P = \log_{10} \frac{p_i}{f_B T} \tag{1.1}$$

where:

- $p_i$ represents the impact probability ;
- T is the time interval (in years) from the possible collision;
- $f_b$ is the background impact frequency depending by the kinetic energy of the asteroid.

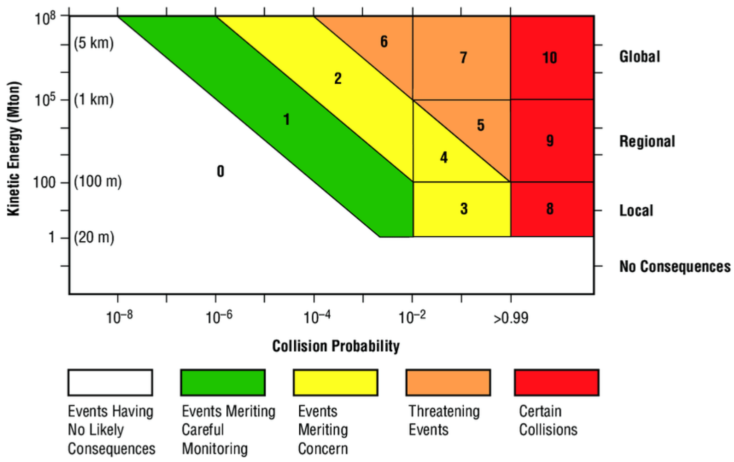


Figure 1.4: the Torino scale [19]

### 1.2.1 The Asteroid Apophis

Apophis (99942) is a near earth asteroid of the Athens class, with an estimated diameter of 370 meters, discovered in 2004. It became famous because it was the first asteroid to receive a rating, in the Torino scale, above 1, with an impact possibility of 1 in 233 on 13/4/2029. Subsequently, with more observations, the probability impact has been updated to 1 in 62, with an update in the Torino scale rating of 4 to then pass today to a value of 0. It was evaluated from the last predictions that on 13/4/2029 Apophis will pass at distance from Earth of 30.000 km (closer than geosynchronous satellites); this flyby will change the asteroid's orbital energy and therefore the orbit itself, passing from an athens-type to an apollos-type orbit (as we can see in figure 1.5 ). This flyby in 2029 will turn the well determined orbit to a poorly known orbit where even small perturbations have an important role. In 2006 was demonstrated that YORP and Yarkovsky effects can affect Apophis post-2029 orbit prediction with a possible impact risk on 13/4/2036 with a value of 1 in the Torino scale. Unfortunately we don't have enough physical data about Apophis to predict exactly the post-2029 orbit with the Yarkovsky and YORP effects. To obtain these data it is necessary a space mission which will rendezvous Apophis analysing its surface and detecting its chemical properties.

| | a (AU) | e | i (deg) | $\omega$(deg) | $\Omega$(deg) |
|---|---|---|---|---|---|
| Before 13/4/29 | 0.922 | 0.191 | 3.331 | 126.402 | 204.446 |
| After 13/4/29 | 1.104 | 0.189 | 2.208 | 71.155 | 203.532 |

Table 1.1: Apophis orbital parameters before and after Earth's flyby on 13/4/2029.

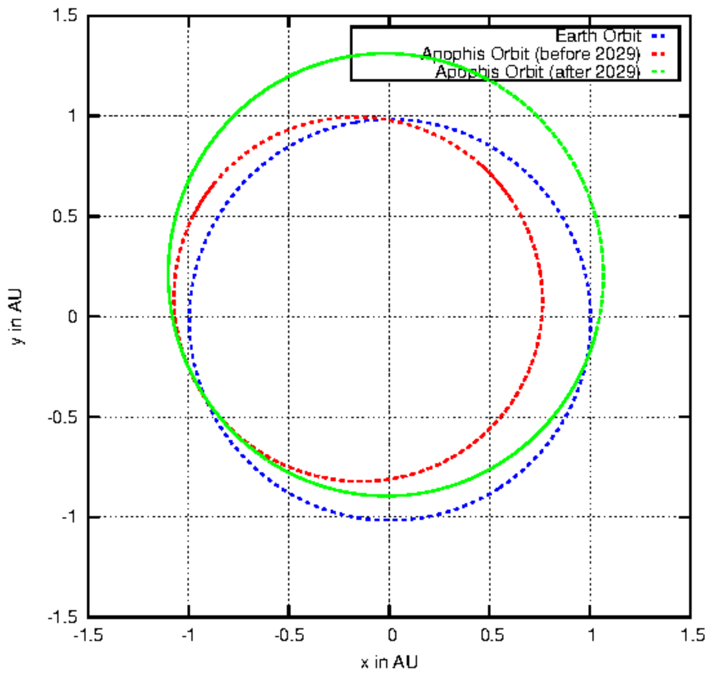


Figure 1.5: Apophis trajectories before and after 2029.[17]

### 1.2.2 The Yarkovsky and YORP effects

Yarkovsky and YORP effects are non gravitational perturbations acting on a rotating celestial body, typically for small asteroids (dimensions $< 10km$) where the effect can't be negligible.

The Yarkovsky effect acts on the perturbation of the semi-major axis changing even the orbital period and is based on the notion that the illuminated surface of an asteroid is heated by the sun and cools down during the night when is not exposed to the sunlight. Because of this phenomenon the asteroids tend to emit a greater amount of heat from the illuminated surface, practically the hottest part of the cosmic object radiates more energy than the coldest part. The difference in radiation emission induces a force that acts on the asteroid in a particular direction that depends on the orientation of the rotation axis and the sense of spin. The obtained force intensity depends on thermal capacity, the albedo and the surface characteristics. This phenomenon was measured for the first time on the asteroid 6489 Golevka, recently the effect was measured again for the asteroids 2009 BD and 2012 LA.

The YORP effect is an extension of the more well-known Yarkovsky effect to include other factors, in addition to the radiation of heat absorbed by the sun, which influence the variation of the rotation speed of the small bodies of the solar system, such as asteroids. The presence of a thermal gradient generates a torque acting on the rotating velocity of the asteroid and its rotating inclination, which modify the Yarkovsky perturbation itself. Confirmation of the existence of the YORP effect has come from various studies conducted in 2007 in two small asteroids, 2000 PH5 and 1862 Apollo), the first was later renamed 54509 YORP to celebrate the positive result obtained.

These effects can modify the asteroids' orbit elements, and it's very difficult to evaluate them because they depend from physical characteristics, which are different for each asteroid. In trajectories evaluations for asteroids with an Earth impact risk, these effects can become fundamental.

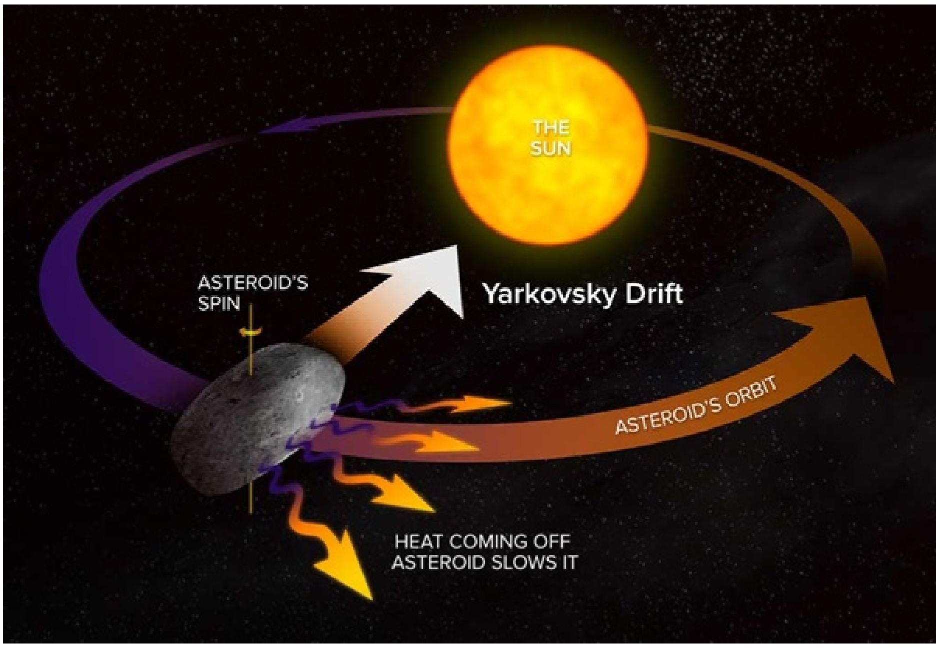


Figure 1.6: The Yarkovsky Effect.[20]

### 1.2.3 The NEST Mission

The Nest mission is a proposal, by the italian astrophysics institute (INAF), for the ESA fast mission opportunity call. The purpose is to rendezvous with multiple near Earth asteroids to understand the evolution of the solar system. These asteroids have in fact different physical properties, ranging from carbonaceous to siliceous, from metallic to basaltic; different compositions implies different formation histories with different internal structures. Moreover these information can be very useful to decrease the NEO risk of impact with the Earth; in fact a monolithic asteroid and a rubble-pile asteroid (gravitational aggregate of fragments) of the same dimension and composition can have different reactions to non-gravitational perturbations (solar pressure and Yarkovsky/YORP effects for example) and to atmospheric re-entry.

Today they are taking place two space missions to near Earth asteroids, the JAXA mission Hayabusa 2 to the asteroid Ryugu and the NASA mission OSIRIS-REx to the asteroid Bennu;the first analysis suggested that still exist big gaps in our asteroids knowledge and their history formation, it's therefore necessary to increase the number of space mission through the asteroids in the future.

The main objectives of the NEST mission are here summarized:

- Understand the initial conditions of the protoplanetary disk and the machanism of formation of terrestrial planets;
- Understand the internal structure of the asteroids with different dimensions;
- Understand the nature of the asteroid Apophis, which has multiple impact risks with the Earth in the next century.

The mission is scheduled for 2028 and will be sent into orbit with the Ariel mission with an Ariane 6 rocket. After that the spacecraft will escape from L2 and will reach the first asteroid (to be determined) with a stay time for the analysis of two months, after that the S/C will start its journey to the main target Apophis. A daughtercraft will be released from the mothercraft, reaching the Apophis' surface and studying its chemical and thermal properties. There is the possibility to reach another asteroid when the Apophis analysis will be finished. An ion electrical thruster is employed and a wet mass of 850 kg is considered.

In this thesis we will individuate the optimal trajectories for the NEST mission, choosing the best asteroids, the duration time and Earth departure date. It is necessary to specify that, apart from the main objective Apophis, the choice of asteroids is not definitive but can be updated in the future thanks to new future NEOs discoveries. In fact the selection of electric propulsion can give more flexibility in launch date, duration , asteroid selections and fuel consumption.

# Chapter 2

# Physical Model

## 2.1 The Two Body Problem

To describe the motion of the spacecraft around the sun we use the Two Body Problem Theory, which is a simplification of the more general N-Body Problem. In particular the theory assumes:

- The presence of two bodies, attracting each other, with a body much greater than the other ($M_1 >> m_2$);
- The bodies are spherically symmetric, they can be treated as point masses;
- There are no external forces acting on the system, a part the two bodies gravitational forces;

This model provides good solutions for spacecrafts' motion around the Sun or planets, but it doesn't consider gravitational perturbation by other bodies.

Applying the Newton's Laws of dynamics is possible to obtain the following differential equation:

$$\ddot{\mathbf{r}} = -\frac{\mu}{r^3}\mathbf{r} \tag{2.1}$$

which describes the motion of the mass $m_2$ respect to the mass $M_1$; $\mu$ represents the gravitational parameter of the attracting body $M_1$, which is product of Gravitational Constant $G$ and the mass $M_1$ , $r$ is the distance between $M_1$ and $m_2$.

| Celestial Body | $\mu$ $[km^3 s^{-2}]$ |
|---|---|
| Sun | $132.712 \times 10^9$ |
| Earth | 398.600 |
| Moon | 4.902 |
| Mars | 42.828 |
| Jupiter | $126.686 \times 10^6$ |

Table 2.1: Gravitational Parameter for different celestial bodies

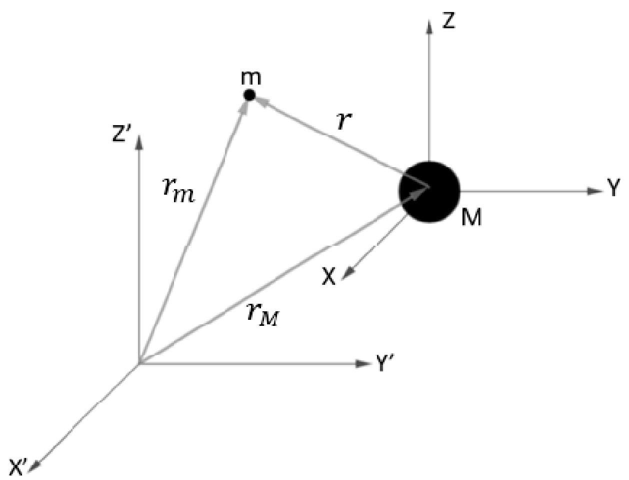


Figure 2.1: Two Body Problem Configuration

### 2.1.1 Mechanical Energy

The gravitational field, generated by the body $M_1$, is conservative. That means the object moving under the gravity of $M_1$ can't gain or lose mechanical energy but can transform kinetic energy to potential energy and vice versa. In orbital mechanics the specific energy (energy per unit mass) is considered and its described by the equation:

$$E = \frac{V^2}{2} - \frac{\mu}{r} = constant \tag{2.2}$$

The equation tell us that, along the orbit, at great distances there are small velocities and at small distances there are great velocities.

### 2.1.2 Angular Momentum

The gravitational force is a force directed radially toward the center of the large body, so there is no change in the angular momentum, in fact to change the angular momentum is necessary a force with tangential component. In orbital mechanics the specific angular momentum is considered and is described by equation:

$$\mathbf{h} = \mathbf{r} \times \mathbf{V} = constant \tag{2.3}$$

The specific angular momentum is the cross product of the position and velocity vectors, and its always perpendicular to the plane containing $\mathbf{r}$ and $\mathbf{V}$. But $\mathbf{h}$ is constant so the position and velocity vectors remain in the same plane, which is called the orbital plane.

### 2.1.3 Trajectory Equation

To obtain the trajectory equation it is necessary integrate equation 2.1 twice, and considering also equations 2.2 and 2.3 we obtain:

$$r = \frac{h^2/\mu}{1 + e\cos\nu} \tag{2.4}$$

where e is the eccentricity orbit value and $\nu$ is the angle between the position vector $\mathbf{r}$ and the periapsis. By varying the angle $\nu$ is possible to obtain all the spacecraft position $\mathbf{r}$.

The equation 2.4 is similar to a conic section equation in polar coordinates with the centre in one of the foci:

$$r = \frac{p}{1 + e\cos\nu} \tag{2.5}$$

where $p$ is the semilatus rectum.

### 2.1.4 Conic Sections

The similarity of the last two equations verifies the Kepler's first law and adds the possibility to include orbital motion along any conic section.There are four types of conic sections and they differ by the eccentricity value $e$.

- $e = 0$ : Circular orbit;
- $0 < e < 1$ Elliptical orbit
- $e = 1$ Parabolic orbit
- $e > 1$ Hyperbolic orbit

Each conic section has two foci and in one of them is located the attracting body. The lenght of the chord passing through the foci is the major axis $2a$, instead $a$ is the semi-major axis; it has positive values for circular and elliptical orbits, negative values for hyperbolic orbits and infinite value for parabolic orbits. The distance between the foci is indicated $2c$ and for circle orbits is equal to zero, for parabola is infinite and for hyperbola is negative. With this two parameters is possible to obtain the orbit eccentricity :

$$e = \frac{c}{a} \tag{2.6}$$

The extreme end-points of the major axes are the periapsis and apoapsis, in particular the periapsis is the nearest point of the orbit to the attracting body, the apoapsis is the furthest point of the orbit. These two distances can be obtained simply inserting $\nu = 0°$ and $\nu = 180°$ in the equation 2.4.

The orbit type can also be evaluated using the Specific Energy, in fact from the Two Body Problem theory is possible to demonstrate that the specific energy is proportional to the semi-major axes of the orbit, and get the following equation:

$$E = -\frac{\mu}{2a} \tag{2.7}$$

| Orbit Type | a | e | Energy |
|---|---|---|---|
| Circular | $> 0$ | 0 | $< 0$ |
| Elliptical | $> 0$ | $< 1$ | $< 0$ |
| Parabolic | $\infty$ | 1 | 0 |
| Hyperbolic | $< 0$ | $> 1$ | $> 0$ |

Table 2.2: Orbit types characteristics.

An overview of the orbit types is summarized in table 2.2.

### 2.1.5 Orbital Parameters

Considering an inertial reference system (X,Y,Z), it is possible to describe the orientation, the size and shape of an orbit with five quantities called "orbital elements", and one quantity to describe the spacecraft position:

- the semi-major axis $a$ : it defines the orbit size;
- the eccentricity $e$ : it defines the orbit shape;
- the inclination $i$ : is the angle between the Z-axis and the angular momentum vector **h**, it represents the inclination between the orbital plane and X-Y plane;
- the longitude of the ascending node $\Omega$ : it is the angle between the X-axis and the point where the spacecraft crosses the fundamental plane in northerly direction, the ascending node, measured counterclockwise.
- the argument of periapsis $\omega$ : is the angle in the orbit plane between the ascending node and the periapsis;
- the true anomaly $\nu$ : it represents the spacecraft position along the orbit for a particular time t , it is the angle in the orbital plane between the spacecraft position and the periapsis;

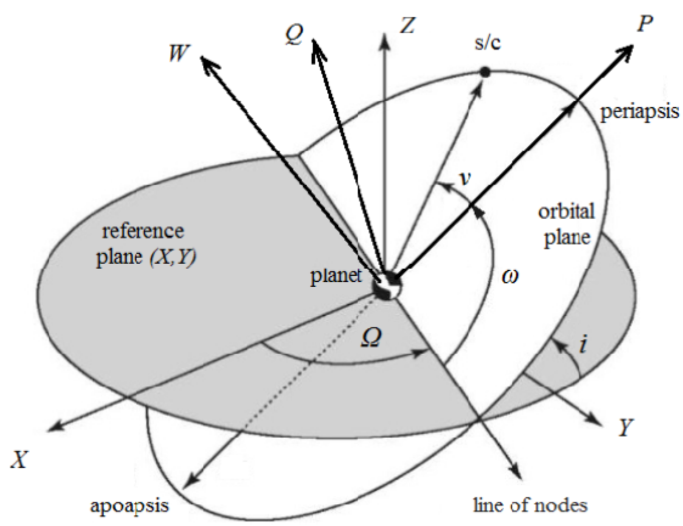


Figure 2.2: Classical orbit elements.

In particular cases, some of these parameters are not defined, for example in circular orbits the argument of periapsis doesn't exist, to determine the spacecraft position is used the argument of latitude $\theta$, which is the angle in orbital plane between the spacecraft and the ascending node. With equatorial orbits instead the position is described by the true longitude $l$, which is the angle between the X-axis and the spacecraft.

These parameters definitions are valid for inertial reference systems like the geocentric-equatorial system or the heliocentric system, only the definitions of the fundamental plane and the axes are different.

## 2.2 Space Propulsion

Propulsion is essential in space trajectories, it permits to make maneuvers and change the spacecraft's orbital parameters. In general the flight of a spacecraft is described by the the equation of motion:

$$m\dot{\boldsymbol{V}} = \dot{m}_p\boldsymbol{c} + \boldsymbol{F_g} \tag{2.8}$$

where:

- $\dot{\boldsymbol{V}}$ is the acceleration vector;
- $\dot{m}_p$ is the propellant mass flow rate;
- $\boldsymbol{c}$ is the exhaust velocity;
- $\boldsymbol{F_g}$ is the local gravitational force

the first term on the right is identified as the thrust of the spacecraft:

$$\boldsymbol{T} = \dot{m}_p\boldsymbol{c} \tag{2.9}$$

and integrating the equation over the complete mission time we obtain the total impulse:

$$I = \int_{t_0}^{t_f} T dt \tag{2.10}$$

To obtain a velocity variation is necessary to vary the spacecraft mass, expelling the propellant in the opposite direction and, in particular in high specific impulse missions, it's preferable achieve the desired thrust with high exhaust velocity and low propellant flow rate instead of low exhaust velocity and high propellant flow rate.

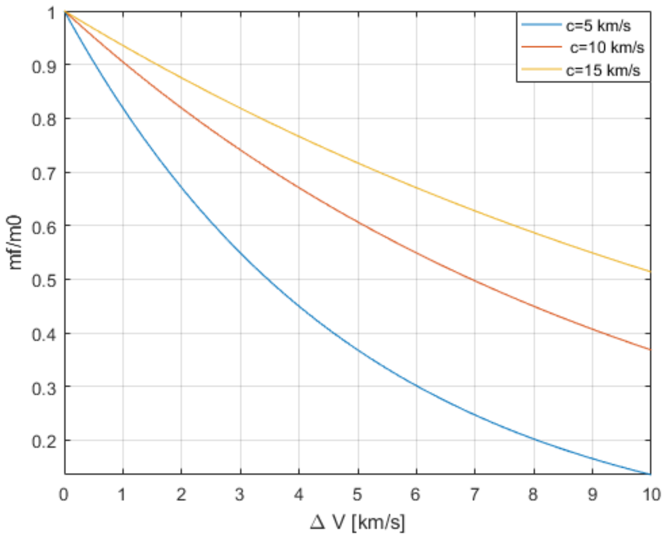


Figure 2.3: Tsiolkovsky equation graph: $\frac{m_f}{m_0}$ trend respect to desired $\Delta V$ considering different exhaust velocities $c$.

Considering an impulse maneuver ($t_f - t_0 \cong 0$) with the absence of gravitational forces, we can integrate equation 2.8 to the scalar form and get:

$$\Delta V = c \ln \frac{m_0}{m_f} \tag{2.11}$$

where $\Delta V$ represents the maximum velocity increment achieved by the ejection of the total propellant, $m_0$ represents the initial mass:

$$m_0 = m_{payload} + m_{structural} + m_{propellant}$$

$m_f$ represents the final mass:

$$m_f = m_0 - m_{propellant}$$

Inverting equation 2.11 we obtain the Tsiolkovsky equation:

$$\frac{m_f}{m_0} = e^{-\frac{\Delta V}{c}} \tag{2.12}$$

It's important to notice that the obtained $\Delta V$ was evaluated considering impulsive thrust and absence of gravity losses , in the reality we must consider no impulsive thrust, gravitational and misalignment losses, with an increase of the real $\Delta V$.

As we can see in figure, 2.3 as the $\Delta V$ increases the final mass decreases,with more propellant consumption, but increasing the exhaust velocity $c$ is possible to obtain larger $\Delta V$ values with the same final mass or larger final mass, for the same $\Delta V$ value.

The propellant exhaust velocity $c$ depends by the nature of acceleration of the propellant gas in the spacecraft's nozzle. It depends to the specific impulse,which is the ratio of thrust to the rate of use of propellant by sea-level weight:

$$I_s = \frac{\dot{m}c}{\dot{m}g_0} = \frac{c}{g_0} \tag{2.13}$$

This parameter represents the efficiency of the propellant; high values of $I_s$ indicates high values of exhaust velocity $c$ and lower propellant consumption.

### 2.2.1 Chemical Thruster

In classical chemical rockets, the thrust is obtained by the propellant expansion in the nozzle, previously heated by the chemical reaction in the combustion chamber. Considering the first principle of thermodynamics:

$$\dot{m}(h_c - h_0) = \dot{m}_p E_{ch} \tag{2.14}$$

where $h_0$ and $h_c$ are the initial and chamber enthalpy respectively, and $E_{ch}$ is the chemical propellant energy per mass produced in the reaction. Considering that the total enthalpy is constant we have :

$$\dot{m}(h_e + \frac{u_e^2}{2} - h_c) = 0 \tag{2.15}$$

where $h_e$ is the enthalpy at the nozzle exit and can be considered negligible. From the last equation we can get:

$$c = u_e = \sqrt{2\eta h_c} = \sqrt{2\eta E_{ch}} = \sqrt{2\eta c_p T_c} \tag{2.16}$$

where $\eta$ represents losses during the nozzle expansion (thermal dispersion, flow misalignment and frozen flow losses), $c_p$ represents the specific heat coefficient and $T_c$ the combustion chamber temperature.

From equation 2.16 we can see the exhaust velocity is limited by the reaction energy and by the maximum tolerable temperature in the combustion chamber. With this limitations it's impossible to obtain high specific impulses and exhaust velocities. In table 2.3 are summarized the performances of the more common chemical propellants.

To obtain higher exhaust velocities is evident that the simple propellant heating is not sufficient. In the electric thruster, the acceleration mechanism

| Propellants | Specific Impulse [s] |
|---|---|
| LOX/LH2 | 400-450 |
| LOX/RP-1 | 300-330 |
| LOX/CH4 | 280-310 |
| NTO/Hydrazine | 280-310 |
| NTO/MMH | 280-310 |
| NC/NG | 200/250 |
| AP/PBAN/Al | 260-290 |

Table 2.3: Tipical Specific Impulse values for chemical rockets

is accomplished by an external agent, which eliminates the relation between propellant used and specific impulse obtained like in the chemical thruster.

### 2.2.2 Electrical Thruster

In the electrical thrusters is necessary electrical power which provides power $P_E$ to the propellant; the obtained power is converted to kinetic energy:

$$\dot{m}(h_e + \frac{u_e^2}{2} - h_0) = \eta P_E \tag{2.17}$$

and we obtain:

$$c = u_e = \sqrt{2\eta \frac{P_E}{\dot{m}_p}} \tag{2.18}$$

Considering that $T = \dot{m}_p c$ equation 2.18 can be rewritten as:

$$c = 2\eta \frac{P_E}{T} \tag{2.19}$$

From equations 2.18 and 2.19 we can guess that to increase the exhaust velocity $c$ and the specific impulse $I_s$ it's necessary to increase the electrical power, decrease the propellant flow rate or decrease the Thrust. It's important to notice that the electrical power is provided by a power generator (typically solar arrays), which has a mass $m_g$ directly proportional to the required power:

$$m_g = kP_E \tag{2.20}$$

For every space mission with electrical thruster exists an optimal specific impulse which maximize the payload mass and minimize the generator and propellant mass. The optimal specific impulse depends on the required $\Delta V$, the mission duration and the generator's technology level.

Electric propulsion permits to achieve a large range of specific impulse, depending on what type of thruster and power generator are adopted. The electric thruster can be divided in three families:

- Electrothermal thruster : the propellant gas is heated electrically, typically with electrical resistors, and accelerated in the nozzle;
- Electrostatic thruster : the propellant gas is accelerated by the application of electric body forces to ionized particles ;
- Electromagnetic thruster: the propellant gas is accelerated by interactions of magnetic and electric fields.

| Type | Propellants | Specific Impulse [s] | Thrust [N] |
|---|---|---|---|
| Resistojets | $N_2/NH_3/\ N_2H_4/H_2$ | 200-350 | 0.2-0.3 |
| Arcjets | $NH_3/\ N_2H_4/H_2$ | 400-1000 | 0.2-1 |
| Ion Thruster | Hg/Xe | 2000-5000 | $< 0.2$ |
| Hall Thruster | Xe | 1500-2000 | $< 2$ |
| Pulsed Plasma Thruster | Argon | 600-2000 | $< 0.01$ |
| MPD Thruster | Teflon | 2000-5000 | $< 2$ |

Table 2.4: Tipical performance values for electrical thruster

From the table 2.4 we can see that the thrust obtained with electrical thruster is very low; therefore to obtain a great $\Delta V$ is necessary to switch on the engine for a long time (days, months or years), consequently the mission time gets longer but with a considerable propellant savings.

# Chapter 3

# Space Trajectories Optimization

## 3.1 Introduction

An optimization problem consist in seeking a control law that makes a particular performance index maximum or minimum. The propellant consumption has a great influence on the costs of an orbital transfer, it becomes essential to minimize the amount of propellant required for the maneuver or, equivalently, maximize the final mass of the vehicle, fixed the initial one. The optimal problem therefore translates into the search for the strategy that allows the orbital transfer to be carried out by maximizing the mass at the end of the maneuver (but other performance indices, such as for example the maximization of the payload taking into account the weight of the propulsion system, can however be taken into consideration). Analytical solutions for this problem type with orbital transfer can be found for a few simple cases, with great simplifications. To find significant solutions, the optimal problem must be resolved with approximate solutions or with numerical methods. There are three types of numerical methods: direct methods, which it is a parameter optimization and solve it with gradient-based procedures; Indirect Methods, which are based on the optimal control theory and transform the optimization problem in a Boundary Value Problem, solved with the shooting method; Evolutionary algorithms, they start from a large number of solutions which evolve towards the optimal solution.In this thesis we will use the Indirect Methods, they have in fact an high numerical precision and can be found an optimal solution with a limited number of parameters and limited computational cost. On the other hand the convergence region may be quite small, and it's necessary start with a good attempt solution.

## 3.2 Optimal Control Theory

The Optimal Control Theory (OCT), based on variational calculus, is described and summarized in the form that best fits to the application of space trajectories.

The generic system which the optimal control theory is applied is described by a variable state vector $\boldsymbol{x}$; the differential equations which describe the evolution between the initial and final instants (external boundary conditions) are functions of $\boldsymbol{x}$, control vector $\boldsymbol{u}$ and independent variable $t$ (time), and they have the generic form:

$$\frac{d\boldsymbol{x}}{dt} = \boldsymbol{f}(\boldsymbol{x}, \boldsymbol{u}, t) \tag{3.1}$$

It is convenient divide the trajectory into a number $n$ of subintervals, within each of which the variables are continuous. The $j$-th interval begins at $t_{(j-1)_+}$ and ends at $t_{j_-}$ and the values that the variables assume at its extremes are $\boldsymbol{x}_{(j-1)_+}$ e $\boldsymbol{x}_{j_-}$ where - and + respectively indicate the values assumed immediately before or after the point considered: in this way it's possible to take into account any discontinuities in the variables (velocity or mass discontinuity after an impulsive maneuver) and also in time (planet's flyby if the time spent inside the sphere of influence is not neglected ), that apply to the junction points between the various arcs (internal boundary conditions).

Boundary conditions are also imposed which are of mixed type, they involve the state and time variables at the external and internal boundaries both. The conditions imposed are generally non-linear and are expressed as:

$$\boldsymbol{\chi}(\boldsymbol{x}_{(j-1)_+}, \boldsymbol{x}_{j_-}, t_{(j-1)_+}, t_{j_-}) = 0 \, j = 1, ....n \tag{3.2}$$

The optimum problem consists in the research of extremal values (relative maximum or minimum) of a functional that, in its general form, is:

$$J = \varphi(\boldsymbol{x}_{(j-1)_+}, \boldsymbol{x}_{j_-}, t_{(j-1)_+}, t_{j_-}) + \sum_j \int_{t_{(j-1)_+}}^{t_{j_-}} \Phi(\boldsymbol{x}(t), \boldsymbol{u}(t), t) dt \; j = 1, .., n \tag{3.3}$$

The functional $J$ is the sum of two terms: the function $\varphi$, depends on the values assumed by the variables and by the time at the contours, and the integral extended to the whole trajectory of the function $\Phi$, which depends on the time and on the values assumed in each point of variables and controls. It's important to notice that with appropriate auxiliary variables is always possible have $\varphi = 0$ (Lagrange Formulation) or $\Phi = 0$ (Mayer Formulation, here preferred) .

It's useful introduce the Lagrange multipliers, constant $\boldsymbol{\mu}$ associated to the boundary conditions, and the adjoint variables $\boldsymbol{\lambda}$, associated to the state equation, and the functional becomes:

$$J^* = \varphi + \boldsymbol{\mu}^T \boldsymbol{\chi} + \sum_j \int_{t_{(j-1)_+}}^{t_{j_-}} (\Phi + \boldsymbol{\lambda}^T (\boldsymbol{f} - \dot{\boldsymbol{x}}) dt) \; j = 1, ..., n \tag{3.4}$$

The functionals $J$ and $J^*$ depend on the time, on the state variable $\boldsymbol{x}$ and their derivates $\dot{\boldsymbol{x}}$ and on the controls $\boldsymbol{u}$. It's clear that if the boundary conditions and the state equation are satisfied, the two functionals and their extremal values coincide. With integration by parts we eliminate the dependency from the derivates of the variable $\dot{\boldsymbol{x}}$ and we obtain:

$$J^* = \varphi + \boldsymbol{\mu}^T \boldsymbol{\chi} + \sum_j (\boldsymbol{\lambda}_{(j-1)_+}^T \boldsymbol{x}_{(j-1)_+} - \boldsymbol{\lambda}_{j_-}^T \boldsymbol{x}_{j_-}) + \sum_j \int_{t_{(j-1)_+}}^{t_{j_-}} (\Phi + \boldsymbol{\lambda}^T (\boldsymbol{f} - \dot{\boldsymbol{\lambda}}^T \boldsymbol{x}) dt) \tag{3.5}$$

and with differentiation we obtain the first functional variation $\delta J^*$ (square brackets represent a matrix ):

$$\begin{aligned} \delta J^* = &\left( -H_{(j-1)_+} + \frac{\partial \varphi}{\partial t_{(j-1)_+}} + \boldsymbol{\mu}^T \frac{\partial \boldsymbol{\chi}}{\partial t_{(j-1)_+}} \right) \delta t_{(j-1)_+} + \\ &\left( H_{j_-} + \frac{\partial \varphi}{\partial t_{j_-}} + \boldsymbol{\mu}^T \frac{\partial \boldsymbol{\chi}}{\partial t_{j_-}} \right) \delta t_{j_-} + \\ &\left( \boldsymbol{\lambda}_{(j-1)_+}^T \frac{\partial \varphi}{\partial x_{(j-1)_+}} + \boldsymbol{\mu}^T \left[ \frac{\partial \boldsymbol{\chi}}{\partial x_{(j-1)_+}} \right] \right) \delta x_{(j-1)_+} + \\ &\left( -\boldsymbol{\lambda}_{j_-}^T \frac{\partial \varphi}{\partial x_{j_-}} + \boldsymbol{\mu}^T \left[ \frac{\partial \boldsymbol{\chi}}{\partial x_{j_-}} \right] \right) \delta x_{j_-} + \\ &\sum_j \int_{t_{(j-1)_+}}^{t_{j_-}} \left( \left( \frac{\partial H}{\partial \boldsymbol{x}} + \dot{\boldsymbol{\lambda}}^T \right) \delta \boldsymbol{x} + \frac{\partial H}{\partial \boldsymbol{u}} \delta \boldsymbol{u} \right) dt \; j = 1, ..., n \end{aligned} \tag{3.6}$$

where $H$ represents the Hamiltonian of the system:

$$H = \Phi + \boldsymbol{\lambda}^T \boldsymbol{f} \tag{3.7}$$

The necessary optimal condition prescribes the stationary of the functional and therefore the cancellation of its first variation for any choice of variations $\delta \boldsymbol{x}, \delta \boldsymbol{u}, \delta \boldsymbol{x}_{(j-1)_+}, \delta \boldsymbol{x}_{j_-}, \delta t_{(j-1)_+}, \delta t_{j_-}$ compatible with the differential equations and boundary conditions. The introduction of adjoint variables and constants permits to cancel at the same time the coefficient of each of the variations in the equation 3.6, ensuring the stationary of the functional expressed by the condition $\delta J^* = 0$.

Annulling the coefficient of $\delta\boldsymbol{x}e\delta\boldsymbol{u}$ in the integral for each point of the trajectory we obtain the Euler-Lagrange differential equations for the adjoint variables:

$$\frac{d\boldsymbol{\lambda}}{dt} = -\left(\frac{\partial H}{\partial \boldsymbol{x}}\right)^T \tag{3.8}$$

and the algebraic equations for the controls:

$$\left(\frac{\partial H}{\partial \boldsymbol{u}}\right)^T = 0 \tag{3.9}$$

It's interesting to note that the control laws are formerly independent from the research of maximum or minimum of $J$. Particular attention must be paid if one of the controls is subject to a constraint, ie it must belong to a given admissibility domain (for example the thrust module must be between the minimum value 0 and the maximum value $T_{max}$). In the presence of a constraint, the optimal value of the control at each point of the trajectory is that which, belonging to the admissibility domain, makes maximum, if the maximums of J are sought, or minimum, if the minimums are sought, the Hamiltonian (equation 3.7) at that point (Pontryagin Maximum Principle). In practice there are two possibilities:

- the optimal control value is provided by the equation 3.9 if it falls in the admissible domain.
- the optimal control value is at extremes of the domain, and assumes the maximum or minimum value, if the one provided by equation3.9 doesn't fall in the admissible domain

A special case occurs if the Hamiltonian is linear respect to one of the control subject to constraints, in the corresponding equation 3.9 the control doesn't appear explicitly and cannot be therefore determined. In this case there are still two possibilities:

- if in the equation 3.7 the control coefficient is not null, the Hamiltonian is maximized by the maximum value of the control if the coefficient is positive and minimum value if the coefficient is negative (bang-bang control), according with Pontryagin Maximum Principle.
- if in the equation 3.7 the control coefficient is null, it's necessary to impose the annulment of all the coefficient's derivative respect to time, until one of them explicitly shows the control: optimal control is then determined by setting this latter derivative equal to zero.

With the rest of boundary conditions, is convenient refers to the j-th contour, writing for this the conditions that derive from considering it as extreme final of (j-1)-th sub-interval or as initial extreme of the j-th sub-interval; annulling in the order the coefficient of $\delta\boldsymbol{x}_{j_-}$,$\delta\boldsymbol{x}_{j_+}$,$\delta\boldsymbol{t}_{j_-}$, $\delta\boldsymbol{t}_{j_+}$ in equation 3.6 we obtain:

$$-\boldsymbol{\lambda}_{j-}^T\frac{\partial\varphi}{\partial x_{j-}}+\boldsymbol{\mu}^T\left[\frac{\partial\boldsymbol{\chi}}{\partial x_{j-}}\right]=0\ \ j=1,....,n \tag{3.10}$$

$$\boldsymbol{\lambda}_{j+}^T\frac{\partial\varphi}{\partial x_{j+}}+\boldsymbol{\mu}^T\left[\frac{\partial\boldsymbol{\chi}}{\partial x_{j+}}\right]=0\ \ j=0,....,n-1 \tag{3.11}$$

$$H_{j-}\frac{\partial\varphi}{\partial t_{j-}}+\boldsymbol{\mu}^T\frac{\partial\boldsymbol{\chi}}{\partial t_{j-}}=0\ \ j=1,....,n \tag{3.12}$$

$$-H_{j+}\frac{\partial\varphi}{\partial t_{j+}}+\boldsymbol{\mu}^T\frac{\partial\boldsymbol{\chi}}{\partial t_{j+}}=0\ \ j=0,....,n-1 \tag{3.13}$$

Where the subscripts $j_-$ and $j_+$ indicate the values assumed respectively immediately before and after the point j. Eliminating the adjoint constants $\boldsymbol{\mu}$ from the equations 3.10 ÷ 3.13 we have the optimal boundary conditions of the type:

$$\boldsymbol{\sigma}\left(\boldsymbol{x}_{(j-1)_+},\boldsymbol{x}_{j_-},\boldsymbol{\lambda}_{(j-1)_+},\boldsymbol{\lambda}_{(j)_-},t_{(j-1)_+},t_{j_-}\right)=0 \tag{3.14}$$

which, with the assigned conditions of equation 3.2, complete the system of differential equations 3.1 and 3.8

Considering a generic state variable x with particular boundary conditions, the equations 3.10 and 3.11 provide particular optimal conditions for the corresponding adjoint variable $\lambda_x$:

- if the state variable $x$ is explicitly assigned at the initial instant (the vector of the imposed conditions $\boldsymbol{\chi}$ contains the equation $x_0-a=0$ with a an assigned value) there are no conditions on the corresponding adjoint variable;

- if the initial state variable value $x_0$ doesn't appear either in the function $\varphi$ or in the boundary conditions, the corresponding adjoint variable is null at the initial state ( $\lambda_{x_0}=0$);

- if a state variable is continuous and not assigned at the internal point ($\boldsymbol{\chi}$ contains the equation $x_{j+}=x_{j-}$) the corresponding adjoint variable is also continuous ($\lambda_{j+}=\lambda_{j-}$);

- if a state variable is continuous and explicitly assigned in an internal contour ($x_{j+} = x_{j-} = a$) the corresponding adjoint variable has a discontinuity, the value $\lambda_{x_{j+}}$ is independent of $\lambda_{x_{j-}}$ and must be determined by the optimization procedure.

Similarly if $H$ doesn't explicitly depend on time, equations 3.12 and 3.13 provide, in some cases, particular boundary conditions:

- if the initial time $t_0$ doesn't explicitly appear in the boundary conditions and in the function $\varphi$, the Hamiltonian is null at the initial state;
- if the intermediate time $t_j$ doesn't appear explicitly in the function $\varphi$, the Hamiltonian is continuous in $j$ ($H_{j+} = H_{j-}$)
- if the time $t_j$ is explicitly assigned ($t_{j+} = t_{j-} = a$), the Hamiltonian has a "free" discontinuity.

### 3.2.1 Boundary Values Problem

The adopted Indirect Method for the optimization of orbital transfers involves the application of the optimal control theory to the system of equation 3.1 which has boundary conditions dependent on orbits type between which the transfer takes place. The optimal control theory formulates a new system of differential equations at the limits, in which some initial values of the variables are unknown. The solution of this problem is to find out which initial values, by numerically integrating the differential system, satisfy all the boundary conditions, both imposed and optimal. We now describe the BVP resolution method and how the optimal problem is formulated to adapt to its characteristics. The optimal control theory formulates the optimal problem as a mathematical problem subject to differential and algebraic constraints. Since some initial values of state and adjoint variables are unknown, the optimal problem translates into a differential boundary problem (BVP) , with the differential equations 3.1 and 3.8, where the controls are determined by the algebraic equations 3.9, supported by the imposed (3.2) and optimal (3.14) boundary conditions . The problem in question has some peculiarities:

- the integration interval is subdivided into sub-intervals in which the differential equations can have different expression.
- the duration of each subinterval is generally unknown;
- boundary conditions can be non-linear and involve the values of variables both at the external and internal boundaries;

- the variables can be discontinuous to the internal contours and their values after the discontinuity can be unknown.

The main difficulty of indirect optimization techniques is precisely the solution of the problem to the limits that emerges from their application: the problem for its solution it's therefore an indispensable tool and also there must be a correspondence between its characteristics and those of the problem in question. The BVP solution is obtained by reducing it to a succession of initial values problem that is brought to convergence according to the Newton method.

To resolve the indeterminacy of the duration of each sub-interval, we resort, for the purpose of integration, to the replacement of the independent variable t with a new variable $\epsilon$ defined in the j-th sub-interval through the relation:

$$\varepsilon = j - 1 + \frac{t - t_{j-1}}{t_j - t_{j-1}} = j - 1 + \frac{t - t_{j-1}}{\tau_j} \tag{3.15}$$

where $\tau_j$ is duration(usually unknown) of the sub-interval. In this way the internal and external contours are fixed, thanks to the introduction of the unknown parameters $\tau_j$, and correspond to consecutive integer values of the new independent variable $\varepsilon$. For the description of the method, we refer to the generic system of equations given by 3.1 and 3.8 in which expression 3.9 have been substituted for controls. There is a complex problem in the state and adjoint variables: $\boldsymbol{y} = (\boldsymbol{x}, \boldsymbol{\lambda})$:

$$\frac{d\boldsymbol{y}}{dt} = \boldsymbol{f}^*(\boldsymbol{y}, t) \tag{3.16}$$

It is necessary to keep in mind that, in the problem under consideration, constant parameters also appear, for example the durations of the subintervals j : it is therefore useful to refer to a new vector $\boldsymbol{z} = (\boldsymbol{y}, \boldsymbol{c})$ which contains the state and adjoint variables and the new vector $\boldsymbol{c}$ of the constant parameters. with the change of independent variable, the system of differential equations is:

$$\frac{d\boldsymbol{z}}{d\varepsilon} = \boldsymbol{f}(\boldsymbol{z}, \varepsilon) \tag{3.17}$$

Modifying the second member of the equations 3.17, we have for the state and adjoint variables:

$$\frac{d\boldsymbol{y}}{d\varepsilon} = \tau_j \frac{d\boldsymbol{y}}{dt} \tag{3.18}$$

and for the constant parameters we have obviously:

$$\frac{d\boldsymbol{c}}{d\varepsilon} = 0 \tag{3.19}$$

The boundary conditions generally are expressed, without distinguishing between imposed and optimal conditions, such as:

$$\boldsymbol{\Psi}(\boldsymbol{s}) = 0 \tag{3.20}$$

where $\boldsymbol{s}$ is a vector which contains the values that variables take on each contour (internal or external) $\varepsilon = 0, 1, ....., n$ and the unknown parameters.

$$\boldsymbol{s} = (\boldsymbol{y}_0, \boldsymbol{y}_1, ......., \boldsymbol{y}_n, \boldsymbol{c}) \tag{3.21}$$

The initial values of some of the variables are generally unknown, the search of solution translates into determining, through an iterative procedure, which values must assume to satisfy the equations 3.20. The r-th iteration starts with the integration of equations 3.17 with the initial values $\boldsymbol{p}^r$ founded on the last iteration:

$$\boldsymbol{z}(0) = \boldsymbol{p}^r \tag{3.22}$$

and we proceed to the integration of the equations along the whole trajectory taking into account any discontinuities in the internal contours. In each contour, the value of the state variables is determined and at the end of integration the error on the boundary conditions $\boldsymbol{\Psi}^r$is evaluated. A variation $\Delta\boldsymbol{p}$ leads to varying the error on the boundary conditions of a quantity which , taking into account only first order terms, is equal to:

$$\Delta\boldsymbol{\Psi} = \left[\frac{\partial\boldsymbol{\Psi}}{\partial\boldsymbol{p}}\right]\Delta\boldsymbol{p} \tag{3.23}$$

Having to cancel the error on the boundary conditions ($\Delta\boldsymbol{\Psi} = -\boldsymbol{\Psi}^r$) in every iteration the initial values are corrected of a quantity:

$$\Delta\boldsymbol{p} = \boldsymbol{p}^{r+1} - \boldsymbol{p}^r = -\left[\frac{\partial\boldsymbol{\Psi}}{\partial\boldsymbol{p}}\right]^{-1}\boldsymbol{\Psi}^r \tag{3.24}$$

until the boundary conditions (equations 3.20) are verified with the desired precision. The matrix that appears in equation 3.24 can be evaluated numerically with a variation of $\boldsymbol{p}$ and integration of equations 3.17. with this procedure is possible evaluate the variation to the boundary conditions $\Delta\boldsymbol{\Psi}(\Delta p)$ obtaining the matrix.

The integration of the differential equations is performed with a variable step and order method based on Adams formulas.

The introduced linearization to evaluate the correction $\Delta\boldsymbol{p}$ of equation 3.24, introduces some errors which can compromise the solution convergence, increasing the error on the boundary condition instead of decreasing it: some precautions have been taken to improve the procedure.

- To avoid moving too far away from the solution, the correction made is a fraction of the one determined:

$$\boldsymbol{p}^{r+1} = \boldsymbol{p}^r + K_1 \Delta \boldsymbol{p} \tag{3.25}$$

  with $K_1 = 0.1 \div 1$, empirical values evaluated during the first codes tests

- At each iteration, after the determination of new vector $\boldsymbol{p}^{r+1}$ with equation 3.25, the maximum error on the boundary conditions $E^{r+1}_{max}$ is compared with the maximum error obtained at the previous iteration $E^r_{max}$: if the maximum error is less than a multiple of the previous one, $E^{r+1}_{max} < K_2 E^r_{max}$, we can proceed with a new iteration. In order to converge to the solution, the error on the boundary conditions can increase in the first iteration, so the value of $K_2$ must be greater than the unit; a value $K_2 = 2 \div 3$ guarantees good results.

- if instead the new iteration error is too large compared to the previous one, we proceed to the bisection of the correction, we integrate the equations of motion with the values:

$$\boldsymbol{p}^{r+1} = \boldsymbol{p}^r + K_1 \Delta \boldsymbol{p}/2 \tag{3.26}$$

  then repeating the comparison between the new maximum error obtained and that of the previous iteration and, if necessary, repeating the bisection. A maximum number of five bisections has been set, after that the process stops, meaning that the attempt solution can't converge.

# Chapter 4

# Problem Definition

To describe the optimal trajectories solutions, the inertial heliocentric reference system is considered and the two body problem equations are used to describe the motion of the spacecraft along the asteroids. The differential equations of motion are:

$$\frac{d\boldsymbol{r}}{dt} = \boldsymbol{V} \tag{4.1}$$

$$\frac{d\boldsymbol{V}}{dt} = -\frac{\mu_\odot}{r^3}\boldsymbol{r} + \frac{\boldsymbol{T}}{m} \tag{4.2}$$

$$\frac{dm}{dt} = -\dot{m} \tag{4.3}$$

where $\boldsymbol{r}$ is the position vector, $\boldsymbol{V}$ is the velocity vector, $\mu_\odot$ is the sun gravitational parameter and $\boldsymbol{T}$ is the Thrust vector, our control variable. The thrust magnitude is dependent by the power available from the solar panels by the relation:

$$T = \frac{2\eta P}{c} \tag{4.4}$$

where $\eta$ is the thruster efficiency and $c$ is the specific impulse, assumed constant. The Power available $P$ as well is influenced by the spacecraft distance from the Sun, assuming an available power of 4.2 kW for a distance of 1 AU, the equation of available power becomes:

$$P = \frac{4.2}{\boldsymbol{r}^2}\,kW \tag{4.5}$$

where $\mathbf{r}$ is the position vector in AU.

| $S_F$ | Thrust |
|---|---|
| $< 0$ | 0 |
| $> 0$ | $T_{max}$ |

Table 4.1: Switching Function

With the state equations is possible to determine the Hamiltonian $H$:

$$H = \boldsymbol{\lambda}_{\boldsymbol{r}}^T \boldsymbol{V} + \boldsymbol{\lambda}_{\boldsymbol{V}}^T \left( \boldsymbol{g} + \frac{\boldsymbol{T}}{m} \right) - \lambda_m \dot{m} \tag{4.6}$$

and can be reformulated:

$$H = \boldsymbol{\lambda}_{\boldsymbol{r}}^T \boldsymbol{V} + \boldsymbol{\lambda}_{\boldsymbol{V}}^T \boldsymbol{g} + T S_F \tag{4.7}$$

where $S_F$ represents the Switching Function:

$$S_F = \frac{\boldsymbol{\lambda}_{\boldsymbol{V}}^T \boldsymbol{T}/T}{m} - \lambda_m \frac{\dot{m}}{T} \tag{4.8}$$

The optimal control must maximize $H$ and the thrust must be parallel to the adjoint vector $\boldsymbol{\lambda}_{\boldsymbol{V}}$:

$$S_F = \frac{\lambda_V}{m} - \lambda_m \frac{\dot{m}}{T} \tag{4.9}$$

It's clear that the maximization of the Hamiltonian depends from the sign of the Switching Function $S_F$. When $S_F > 0$ is convenient to have maximum thrust, whereas is convenient have zero thrust when $S_F < 0$.

## 4.1 State and Adjoint equations

Referring to an inertial reference system centered in the Sun with spherical coordinates: the spacecraft's position is described by the radius $r$, longitude $\vartheta$ and latitude $\phi$.

$$\boldsymbol{r} = \begin{bmatrix} r \\ \vartheta \\ \phi \end{bmatrix}$$

The spacecraft velocity is described by a local reference system with the radial component $u$, in east direction $v$ and north direction $w$.

$$\boldsymbol{V} = \begin{bmatrix} u \\ v \\ w \end{bmatrix}$$

The state equations in the considered reference system are:

$$\frac{dr}{dt} = u \tag{4.10}$$

$$\frac{d\vartheta}{dt} = \frac{v}{rcos\phi} \tag{4.11}$$

$$\frac{d\phi}{dt} = \frac{w}{r} \tag{4.12}$$

$$\frac{du}{dt} = -\frac{\mu}{r^2} + \frac{v^2}{r} + \frac{w^2}{r} + \frac{T}{m}sin\gamma_T \tag{4.13}$$

$$\frac{dv}{dt} = -\frac{uv}{r} + \frac{vw}{r}\tan\phi + \frac{T}{m}\cos\gamma_T\cos\psi_T \tag{4.14}$$

$$\frac{dw}{dt} = -\frac{uw}{r} - \frac{v^2}{r}\tan\phi + \frac{T}{m}\cos\gamma_T\sin\psi_T \tag{4.15}$$

$$\frac{dm}{dt} = -\frac{T}{c} \tag{4.16}$$

where $\gamma_T$ and $\psi_T$ are the the elevation and heading control angles of Thrust $\boldsymbol{T}$ and they determine the Thrust direction. Considering equation 4.6 we can evaluate the Hamiltonian $H$:

$$\begin{aligned} H =& \lambda_r u + \lambda_\vartheta \frac{v}{rcos\phi} + \lambda_\phi \frac{w}{r} + \\ & \lambda_u \left(-\frac{\mu}{r^2} + \frac{v^2}{r} + \frac{w^2}{r} + \frac{T}{m}sin\gamma_T\right) + \\ & \lambda_v \left(-\frac{uv}{r} + \frac{vw}{r}\tan\phi + \frac{T}{m}\cos\gamma_T\cos\psi_T\right) + \\ & \lambda_w \left(-\frac{uw}{r} - \frac{v^2}{r}\tan\phi + \frac{T}{m}\cos\gamma_T\sin\psi_T\right) - \lambda_m\frac{T}{c} \end{aligned} \tag{4.17}$$

From the Optimal Control Theory we can obtain the algebraic equations of controls:

$$\left(\frac{\partial H}{\partial \boldsymbol{u}}\right)^T = 0 \tag{4.18}$$

With the last equation is possible to determine the optimal control values of $\gamma_T$ and $\psi_T$, it is sufficient in fact derive the hamiltonian respect to $\gamma_T$ and $\psi_T$ and set them equal to zero.

$$\frac{\partial H}{\partial \gamma_T} = 0 \tag{4.19}$$

$$\frac{\partial H}{\partial \psi_T} = 0 \tag{4.20}$$

From the last two equations is possible to get the optimal control angles:

$$\sin \gamma_t = \frac{\lambda_u}{\lambda_V} \tag{4.21}$$

$$\cos \gamma_t \cos \psi_T = \frac{\lambda_v}{\lambda_V} \tag{4.22}$$

$$\cos \gamma_t \sin \psi_T = \frac{\lambda_w}{\lambda_V} \tag{4.23}$$

where:

$$\lambda_V = \sqrt{\lambda_u^2 + \lambda_v^2 + \lambda_w^2} \tag{4.24}$$

is the primer vector, parallel to the optimal thrust direction.

Again from the Optimal Control Theory with the Euler-Lagrange equation:

$$\frac{d\boldsymbol{\lambda}}{dt} = -\left(\frac{\partial H}{\partial \boldsymbol{x}}\right)^T \tag{4.25}$$

we can evaluate the differential equations of the adjoint variables:

$$\begin{aligned}\dot{\lambda}_r =& \frac{1}{r^2}[\lambda_\vartheta \frac{v}{\cos\phi} + \lambda_\phi w + \lambda_u \left(-\frac{2}{r} + v^2 + w^2\right) + \\ & \lambda_v \left(-uv + vw \tan\phi\right) + \lambda_w \left(-uw - v^2 \tan\phi\right)]\end{aligned} \tag{4.26}$$

$$\dot{\lambda}_\vartheta = 0 \tag{4.27}$$

$$\dot{\lambda}_\phi = \frac{1}{r\cos^2\phi}\left(-\lambda_\vartheta v \sin\phi - \lambda_v vw + \lambda_w v^2\right) \tag{4.28}$$

$$\dot{\lambda}_u = \frac{1}{r}\left(-\lambda_r r + \lambda_v v + \lambda_w w\right) \tag{4.29}$$

$$\dot{\lambda}_v = \frac{1}{r}\left(-\lambda_\vartheta \frac{1}{\cos\phi} - 2\lambda_u v + \lambda_v(u - w\tan\phi) + 2\lambda_w v \tan\phi\right) \tag{4.30}$$

$$\dot{\lambda}_w = \frac{1}{r}\left(-\lambda_\phi - 2\lambda_u w - \lambda_v v \tan\phi + \lambda_w u\right) \tag{4.31}$$

$$\dot{\lambda}_m = \frac{T}{m^2}\lambda_V \tag{4.32}$$

The obtained state and differential equations are put together into a differential equations system.

## 4.2 Boundary Conditions

Once the differential equations are obtained, it is necessary to impose the boundary conditions. We consider a space mission with a departure from the Earth a the time $t_0$ reaching N asteroids at different times $t_N$. The spacecraft will stay on asteroid two months, for the scientific research, then it will restart towards the next asteroid. The trajectory is divided in N arcs, depending on how many asteroids N we want to reach. For each arc is necessary to impose some boundary conditions, in particular at the time $t_0$ the spacecraft position and velocity must be equal to the Earth position and velocity with an initial mass of 850 kg.

$$\begin{aligned} \boldsymbol{r}_{S/C}(t_0) &= \boldsymbol{r}_{Earth}(t_0) \\ \boldsymbol{V}_{S/C}(t_0) &= \boldsymbol{V}_{Earth}(t_0) \\ m_0(t_0) &= 850\,kg \end{aligned}$$

At the end of the first arc the spacecraft position and velocity must be equal to the first asteroid position and velocity:

$$\boldsymbol{r}_{S/C}(t_1) = \boldsymbol{r}_{Asteroid1}(t_1)$$

$$\boldsymbol{V}_{S/C}(t_1) = \boldsymbol{V}_{Asteroid1}(t_1)$$

At the beginning of the second arc, $t_2$, the spacecraft starts from the first asteroid towards the second, its mass must be equal to the mass at the time $t_1$, while its position and velocity must be equal to the first asteroid position and velocity at $t_2$:

$$\begin{aligned} m(t_2) &= m(t_1) \\ \boldsymbol{r}_{S/C}(t_2) &= \boldsymbol{r}_{Asteroid1}(t_2) \\ \boldsymbol{V}_{S/C}(t_2) &= \boldsymbol{V}_{Asteroid1}(t_2) \end{aligned}$$

At the time $t_3$ the spacecraft reaches the final asteroid and again the spacecraft position and velocity must coincide with those of the final asteroid.

$$\boldsymbol{r}_{S/C}(t_3) = \boldsymbol{r}_{Asteroid2}(t_3)$$
$$\boldsymbol{V}_{S/C}(t_3) = \boldsymbol{V}_{Asteroid2}(t_3)$$

The times $t_0$, $t_1$, $t_2$, $t_3$ can be imposed or be optimized. For time optimization is necessary analyse the Switching Function trend over time, in particular for each arc we analyse the Switching Function at the beginning and at the end. If at the beginning $S_F < 0$, the spacecraft is not thrusting, and it stays in its initial orbit, if at the end $S_F < 0$ the spacecraft is not thrusting again, that means it reaches the asteroid previously. The optimal departure date is when the $S_F$ changes from negative to positive values, and the optimal arrive date is when the $S_F$ changes from positive to negative values.

## 4.3 Initial conditions

Once the boundary conditions are set it's possible to solve the differential equations system. To resolve it, satisfying the boundary conditions, it is necessary start with the right initial conditions, contained in the vector $p$, which are integrated by the differential equations system. For each arc is necessary have an initial conditions vector.

$$\boldsymbol{p} = \begin{bmatrix} t_0 \\ t_f \\ r_0 \\ \vartheta_0 \\ \phi_0 \\ u_0 \\ v_0 \\ w_0 \\ \lambda_{r0} \\ \lambda_{\vartheta 0} \\ \lambda_{\phi 0} \\ \lambda_{u0} \\ \lambda_{v0} \\ \lambda_{w0} \end{bmatrix}$$

Where $t_0$ is the initial departure time from the Earth or from the asteroid (it depends by the arc number), $t_f$ is the arrive time to the asteroid, $r_0$, $\vartheta_0$, $\phi_0$ are the spacecraft initial position, $u_0$, $\vartheta_0$, $w_0$ are the spacecraft initial velocity. While $\lambda_{r0}, \lambda_{\vartheta 0}, \lambda_{\phi 0}, \lambda_{u0}, \lambda_{v0}, \lambda_{w0}$ are the initial adjoint variables. As we have seen before the velocity adjoints variables values determine the optimal Thrust direction:

$$T \sin \gamma_t = T \frac{\lambda_u}{\lambda_V}$$

$$T \cos \gamma_t \cos \phi_t = T \frac{\lambda_v}{\lambda_V}$$

$$T \cos \gamma_t \sin \phi_t = T \frac{\lambda_w}{\lambda_V}$$

which is parallel to the prime vector $\lambda_V$.

Unfortunately at the beginning some or all the vector values are unknown, so the problem translates from a Boundary Value Problem (BVP) to an Initial Boundary Problem (IVP). As we saw in the previous chapter, to solve the problem, the shooting method is adopted, in particular we consider an initial attempt solution $p_0$ and we integrate it with the differential equations systems. After that we compare the obtained results with the boundary conditions to satisfy, if the errors are less then tolerance imposed, the initial values of the problem are found, otherwise is necessary to modify the initial vector $p$ and re-integrating it until the error tolerance is achieved.

When the initial values of each arc are found, we can get the optimal trajectory solution, with the all parameters trend along the time. At the end of each arc, knowing the spacecraft initial and final mass, is possible to obtain, with the Tsiolkovsky equation, the required $\Delta V$:

$$\Delta V = c \ln \frac{m_0}{m_f} \tag{4.33}$$

To resolve the IVP a numerical code was implemented. The code solves the Initial Boundary Value Problem with an indirect method, in figure 4.1 is possible to see the code flow chart, and works with dimensionless parameters, in particular:

- the distances become dimensionless using the Sun-Earth mean distance

$$r_{conv} = 1.4959 * 10^8 \, km$$

- the velocities become dimensionless using the Earth circular velocity:

$$V_{conv} = \sqrt{\frac{\mu_\odot}{r_{conv}}} = 29.784 \, km/s$$

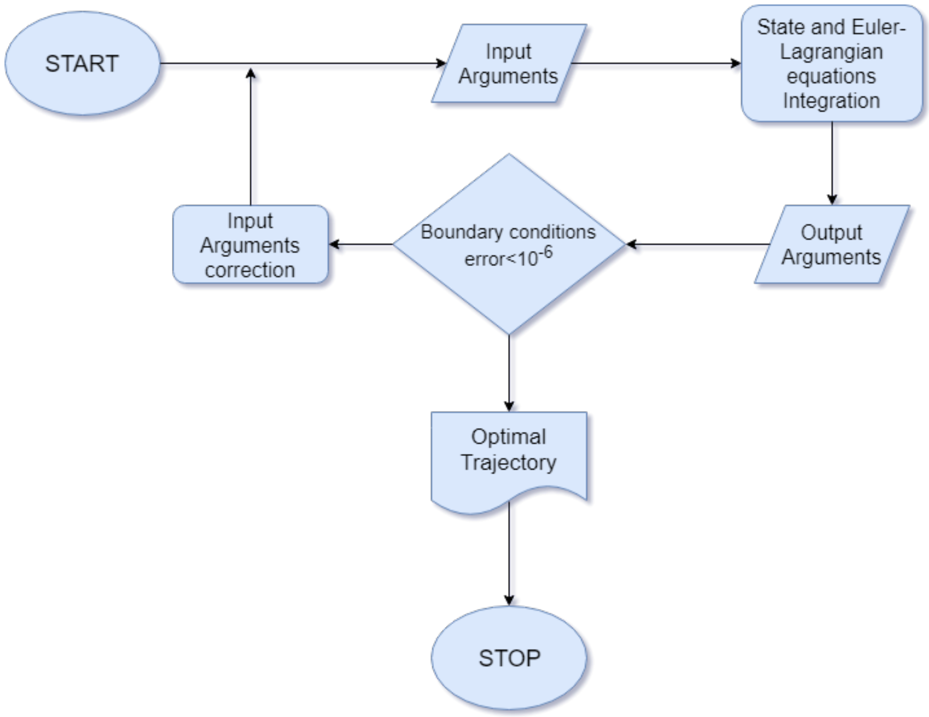


Figure 4.1: Numerical Code Flowchart

- the accelerations become dimensionless using the Earth acceleration around the Sun:

$$a_{conv} = \frac{\mu_{\odot}}{r_{conv}^2} = 5.93 * 10^{-6}\, km/s^2$$

- the time becomes dimensionless using the relation:

$$t_{conv} = \frac{V_{conv}}{a_{conv} * 86400} = 58.1324\, days$$

- the dates are dimensionless and start from 1/1/2000 with a value of 0, to continue then with the time $t_{conv}$. Example $176 = 5/01/2029, 176 + 2\pi = 182.28 = 5/01/2030$

# Chapter 5

# Results

## 5.1 Introduction

The NEST mission aims to rendezvous with multiple near-Earth asteroids, in particular with asteroid Apophis (99942), analyzing the external surfaces, the chemical and thermal properties, the bulk densities to determine the non gravitational effects. The most important perturbation acting on small asteroids is the Solar Radiation Pressure which generates two other non gravitational perturbations: the Yarkovsky and YORP effects. These perturbations can vary the orbital parameters of the body, it's therefore necessary to study these effects to prevent a future Asteroid-Earth Impact.

The proposed mission will start in 2028 and will be released in L2 by Ariel Mission, after that the spacecraft will start its journey to the first asteroid, analyzing it for two months, then it will start again towards the main target Apophis. After two months the mission will continue reaching the last asteroid. The total mission duration should be less than five years.

In this chapter we analyse all the possible trajectories, selecting the best asteroids to reach in terms of duration and $\Delta V$. In this study only the heliocentric phase is considered with a null relative velocity from Earth, and, according with the call specification, a wet mass of 850 kg is considered with 250 kg reserved for propellant. Electric propulsion is employed, using the Ion-thruster Ariane RIT X2, with 3300 s of specific impulse, a nominal Thrust of 160 mN (at 1 AU) and a constant efficiency of 0.625, the power available is $4.2/r^2$ kW (distance from the sun $r$ in AU).

| | |
|---|---|
| Wet Mass | 850 kg |
| Thruster Specific Impulse | 3300 s |
| Nominal Thrust | 160 mN (1 AU) |
| Thruster Efficiency $\eta$ | 0.625 |
| Power Available from solar panels | 4.2 kW (1 AU) |

Table 5.1: Mission Parameters

# 5.2 Asteroid Selection

## 5.2.1 First Asteroid

To evaluate the optimal trajectories we have to select the asteroids first. The selection process was based on the possibility to reach the asteroids quickly with a reduced propellant consumption. To obtain a low propellant consumption with a low duration it's necessary analyse the asteroids' orbital parameters and their phase shift angles with the Earth. After that was done another selection process, based on studies previously done by scientists, who detected the presence of the Yarkovsky and YORP effects. The most interesting asteroids for the mission with their orbital parameters are summarized in Table 5.2.

| Asteroid | $a$(AU) | $e$ | $i$(deg) | $\omega$(deg) | $\Omega$(deg) |
|---|---|---|---|---|---|
| 2009 BD | 1.0097 | 0.0416 | 0.3844 | 109.8709 | 58.1275 |
| 2009 YF | 0.9359 | 0.1213 | 1.5272 | 193.3747 | 87.6164 |
| 2012 LA | 1.0397 | 0.0232 | 3.1212 | 76.8760 | 235.0493 |
| 2013 WA44 | 1.1004 | 0.0604 | 2.3022 | 176.7311 | 56.5129 |
| 2014 QN266 | 1.0526 | 0.0923 | 0.4882 | 61.5896 | 171.1095 |
| 2018 PN22 | 0.9971 | 0.0392 | 4.3849 | 219.176 | 317.0775 |

Table 5.2: Selected Asteroids with Orbital Parameters

For each asteroid were evaluated different trajectories solutions, varying the departure date from Earth and duration period. First of all we selected three possible departure dates across the year 2028: January, June and December, after that we imposed different duration time to reach the first Asteroid,with the constraint to not exceed 24 months. It's clear that a longer journey duration implies a lower propellant consumption and lower $\Delta$V and vice versa. In table 5.3 are summarized the final masses of the S/C after the first trajectory arc with different asteroids on 05/1/28. The tables for departure of June and December are omitted for sake of conciseness. To

| Duration | 2009BD | 2009YF | 2012LA | 2013WA44 | 2014QN266 | 2018PN22 |
|---|---|---|---|---|---|---|
| 8 | / | 0.7884 | 0.7724 | 0.7826 | 0.8008 | 0.7829 |
| 9 | / | 0.7884 | 0.7874 | 0.799 | 0.8008 | 0.7829 |
| 10 | 0.7425 | 0.7884 | 0.7916 | 0.802 | 0.8008 | 0.7838 |
| 11 | 0.7425 | 0.7885 | 0.7943 | 0.802 | 0.8013 | 0.7838 |
| 12 | 0.7449 | 0.7909 | 0.7962 | 0.802 | 0.8049 | 0.7838 |

Table 5.3: S/C final mass for the first trajectory arc: Earth-Asteroid X, with departure date 05/1/28

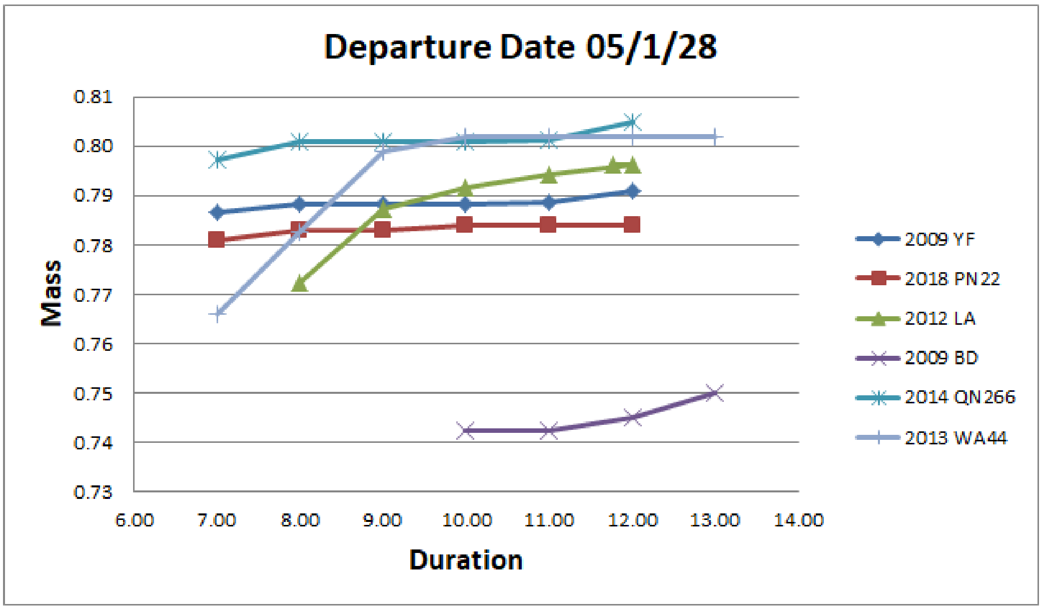


Figure 5.1: S/C mass trend respect to duration for the first trajectory arc: Earth-Asteroid X.

better analyse the mass trend respect to duration a graph was created, fig 5.1; again only the graph with departure date on 05/1/28 is showed for sake of conciseness. The different color lines represent the different asteroids and, as obvious, increasing the duration also increases the final mass.

Once the first object has been reached, it was imposed a stay time of two months for the scientific analysis and, after that, the spacecraft can restart its journey towards the main target Apophis , with a departure date depending on the first arc arrival date.

Also the second arc was calculated with different duration periods and departure dates. In particular for each asteroid, three starting dates (depending on the arrival of the first arc) were considered, generally with an interval of four months from each other, and different duration times, obtaining the final mass and $\Delta V$ consumption. The $\Delta V$ trend respect to time has been plotted again, as can be seen in figure 5.2, the different lines indicate the different starting dates from the asteroid.

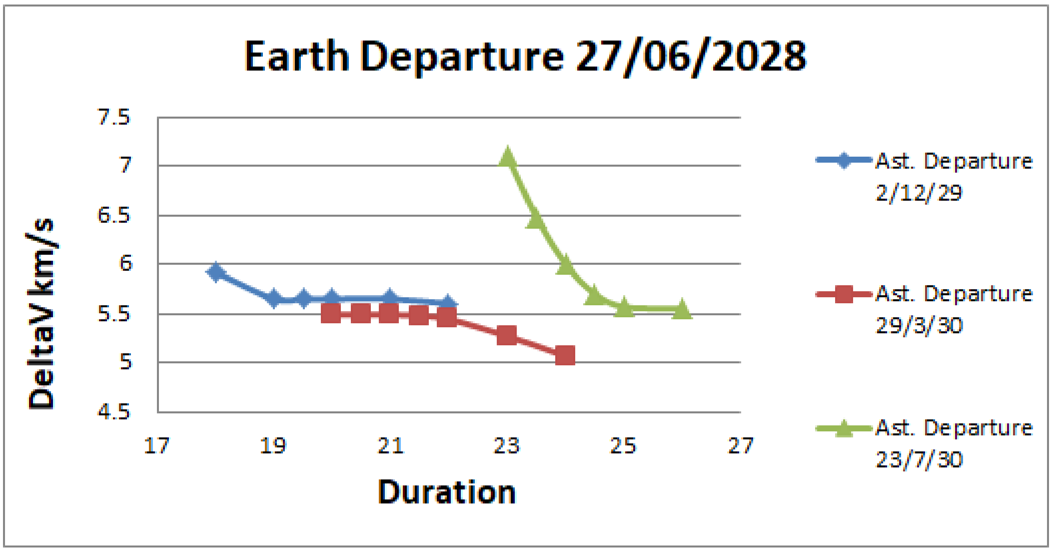


Figure 5.2: $\Delta V$ consumption respect to duration time (in this graph 1 unit=2 months) for the trajectory Earth-2012 LA-Apophis.

Of these three solutions the best one was chosen in terms of $\Delta V$ and duration and compared with the best solutions of other asteroids with the same start from Earth, obtaining the graph in figure 5.3.

Analysing the graph in figure 5.3 and the other graphics, with departure date on January and December (here omitted), the best candidates are the asteroids 2014 QN266 and 2012 LA, they have in fact always (in all the three graphics) the best mass values respect to the other asteroids.

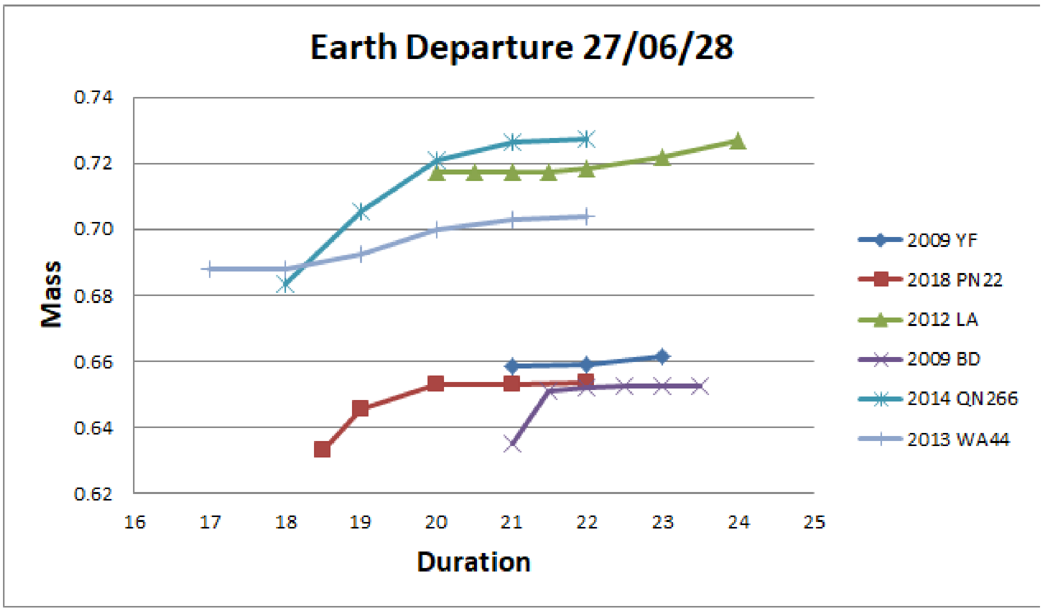


Figure 5.3: Mass trend over duration for different trajectories

As we can see in the figure 5.2 and in tables 5.4,5.5,5.6 the departure date from the first asteroid influences the propellant consumption, and a late departure can improve it considerably. In some cases it is therefore preferable to reach the asteroid first, with a more propellant consumption in the first arc, and then benefit from it in the second arc with a lower total consumption respect to the other cases.

| Earth Departure | 2012LA Arrival | $\Delta V_1$ [km/s] | Duration (Days) |
|---|---|---|---|
| 27/06/28 | 5/10/29 | 2.419 | 465 |
| 27/06/28 | 30/01/30 | 2.259 | 581 |
| 27/06/28 | 26/05/30 | 2.09 | 697 |

Table 5.4: $\Delta V$ consumption of first arc: Earth-2012LA with different durations

| 2012LA Departure | Apophis Arrival | $\Delta V_2$ [km/s] | Duration (Days) |
|---|---|---|---|
| 2/12/29 | 31/10/32 | 3.23 | 697 |
| 29/03/30 | 24/02/32 | 3.01 | 697 |
| 23/07/30 | 20/06/32 | 3.48 | 697 |

Table 5.5: $\Delta V$consumption of second arc: 2012LA-Apophis with equal duration

| Earth Departure | Apophis Arrival | $\Delta V_{tot}$ [km/s] | Duration (Days) |
|---|---|---|---|
| 27/06/28 | 31/10/32 | 5.649 | 1212 |
| 27/06/28 | 24/02/32 | 5.273 | 1336 |
| 27/06/28 | 20/06/32 | 5.57 | 1452 |

Table 5.6: Total $\Delta V$consumption of Earth-2012LA-Apophis.

### 5.2.2 Date departure and duration optimization

All the trajectories analysis were made with an imposed departure date and duration,but with these parameters it's almost impossible find an optimized trajectory. For each trajectory sequence was made an optimization work to minimize the journey duration and propellant consumption, analysing the Switching Function of each solution. The Switching Function (SF) represents the thruster status: SF $> 0$ indicates the thruster is switched on at maximum thrust, SF $< 0$ indicates the thruster is switched off, so with zero thrust. The value of SF can change during the journey in according to the Optimal Control Theory.

| SF | Thrust |
|---|---|
| $< 0$ | 0 |
| $> 0$ | $T_{max}$ |

Table 5.7: Switching function

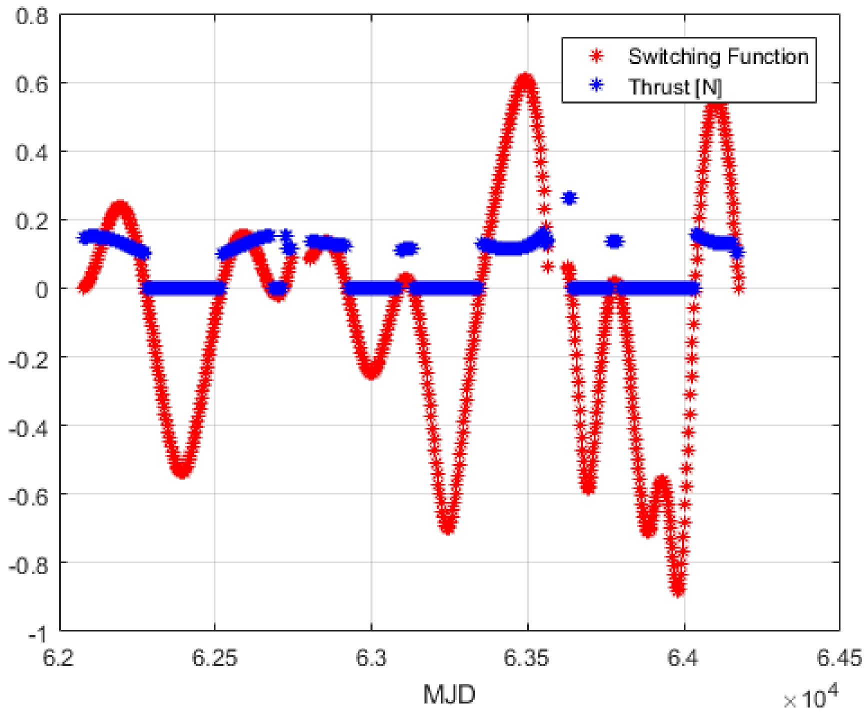


Figure 5.4: Switching Function and Thrust trend, the thrust varies indirectly proportional to the square of the distance from the sun, in according to available power of the solar panels. The duration is represented in Modified Julian Date (MJD)

In figure 5.4 is represented the trend of the SF and Thrust along the time of an hypothetical mission sequence, we can see the Thrust is equal to zero when the SF$< 0$ and Thrust is maximum when SF$> 0$. The optimization process consists to analyse the SF trend and verify the value at the beginning and at the end of the mission.If,at the departure date, the SF$<= 0$, it means that the spacecraft is not thrusting, but it remains in the initial orbit. To evaluate the real departure date it's necessary to check when the SF changes from negative to positive value. The same process was done also for the arrival date; if the SF has negative value,this means that the spacecraft reached the final target previously, and the real duration of the journey is less than the imposed one.A clear example is showed in fig 5.5.At the departure date and at the arrival the SF is $< 0$,this means that the journey start will be later and the arrival will be sooner. With the optimization process the zero thrust start and arrival were eliminated and we obtained a new graph represented in fig 5.6.

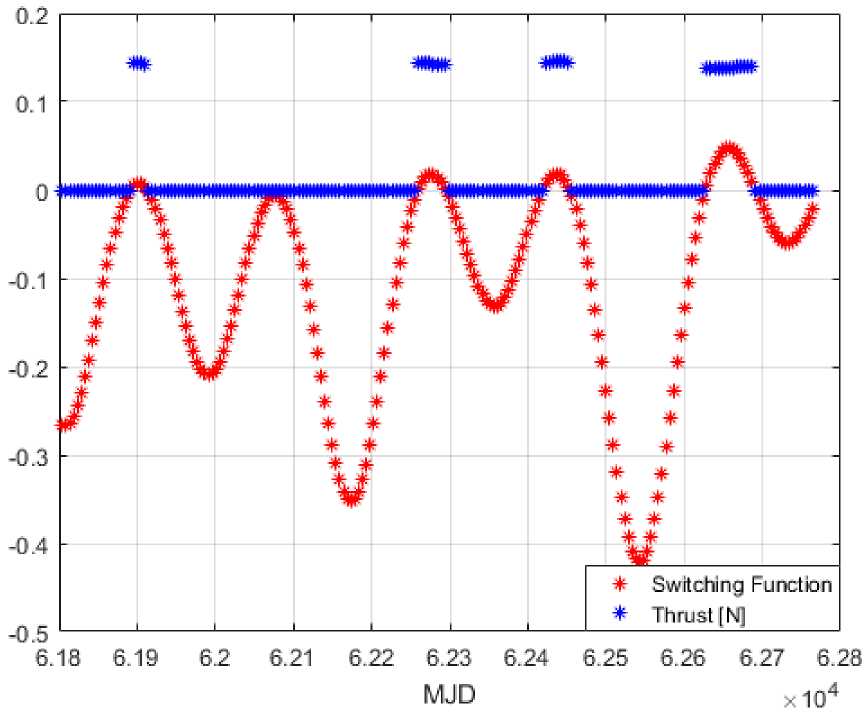


Figure 5.5: Switching Function and Thrust trend of the sequence Earth-2012LA, before optimization.

The optimization process was done for each asteroid and for different departure dates (beginning, mid and end 2028) obtaining the results summarized in tables 5.8, 5.9, 5.10.

Analysing the $\Delta V$ consumption and the duration time ,with the optimization process, again the best asteroids to take in to account, as firs mission target, are 2012 LA and 2014 QN266.

| Earth departure date beginning 2028 | | | | | |
|---|---|---|---|---|---|
| Asteroid | Earth Dep. | Ast. Arr. | Apophis Arr. | ΔV | Mass |
| 2009 BD | 5/1/28 | 30/1/30 | 2/10/31 | 8.331 | 657 |
| 2009 YF | 9/1/28 | 26/2/29 | 22/12/30 | 5.611 | 714 |
| 2012 LA | 5/1/28 | 2/12/29 | 17/6/31 | 5.41 | 719 |
| 2013 WA44 | 23/4/28 | 18/8/29 | 18/1/31 | 6.238 | 703 |
| 2014 QN266 | 5/1/28 | 14/4/29 | 13/11/30 | 5.004 | 728 |
| 2018 PN22 | 5/1/28 | 7/3/29 | 10/7/31 | 7.620 | 671 |

Table 5.8: $\Delta V$ consumption of Earth-Asteroid-Apophis optimized trajectories with departure at beginning 2028.

| Earth departure date mid 2028 | | | | | |
|---|---|---|---|---|---|
| Asteroid | Earth Dep. | Ast. Arr. | Apophis Arr. | ΔV | Mass |
| 2009 BD | 27/6/28 | 14/12/31 | 27/7/32 | 6.729 | 694 |
| 2009 YF | 27/6/28 | 5/10/29 | 31/10/31 | 8.282 | 658 |
| 2012 LA | 27/6/28 | 28/12/29 | 17/6/31 | 5.493 | 717 |
| 2013 WA44 | 27/6/28 | 5/10/29 | 31/10/31 | 6.148 | 703 |
| 2014 QN266 | 27/6/28 | 8/10/30 | 4/12/31 | 5.006 | 728 |
| 2018 PN22 | 12/7/28 | 8/8/29 | 4/8/31 | 8.519 | 653 |

Table 5.9: $\Delta V$consumption of Earth-Asteroid-Apophis optimized trajectories with departure at mid 2028.

| Earth departure date end 2028 | | | | | |
|---|---|---|---|---|---|
| Asteroid | Earth Dep. | Ast. Arr. | Apophis Arr. | ΔV | Mass |
| 2009 BD | 19/12/28 | 20/3/31 | 22/3/32 | 8.042 | 663 |
| 2009 YF | 19/12/28 | 8/12/29 | 29/11/32 | 6.924 | 686 |
| 2012 LA | 4/11/28 | 26/3/30 | 29/6/32 | 4.954 | 729 |
| 2013 WA44 | 19/12/28 | 24/10/30 | 13/3/32 | 7.1058 | 682 |
| 2014 QN266 | 12/11/28 | 4/10/30 | 17/1/32 | 5.746 | 712 |
| 2018 PN22 | 19/12/28 | 10/2/30 | 17/8/32 | 7.869 | 666 |

Table 5.10: $\Delta V$consumption of Earth-Asteroid-Apophis optimized trajectories with departure at end 2028.

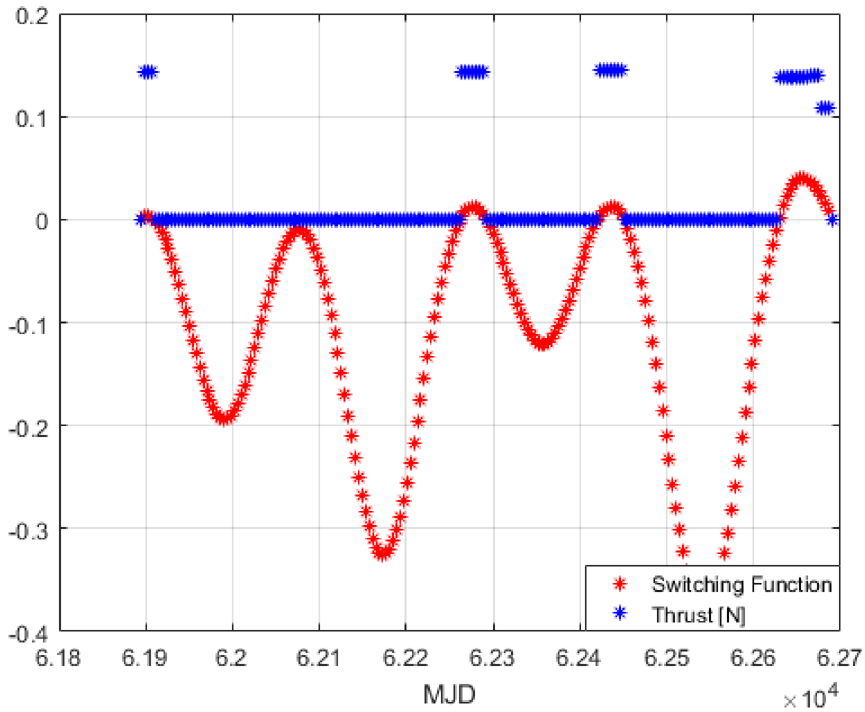


Figure 5.6: Switching Function and Thrust trend of the sequence Earth-2012LA, after optimization.

### 5.2.3 Third Asteroid

Once Apophis has been reached, the mission can have an expansion and reach another Asteroid, if there is enough propellant. The candidate Asteroids are the same of the First Asteroid selection in table 5.2.

To select the best Asteroid we again evaluate different trajectories solutions changing the departure date from Apophis, with an interval of four months from each other, the duration and the third asteroid in the sequence: Apophis - Asteroid X . In figures 5.7and 5.8 are shown different solutions with different departure dates and durations.

Analysing the plots it's clear that the best choice, for the third target, is the Asteroid 2014 QN266, it has always the lowest ΔV consumption in every departure date and for each journey time. Moreover considering that 2014 QN266 and 2012 LA are the best candidate as First Asteroid, and 2012 LA has no good solutions has Third Asteroid, the best Asteroid sequence is Earth - 2012 LA - Apophis - 2014 QN 266; it has the lowest $\Delta V$ consumption respect to other sequence with the same time duration.

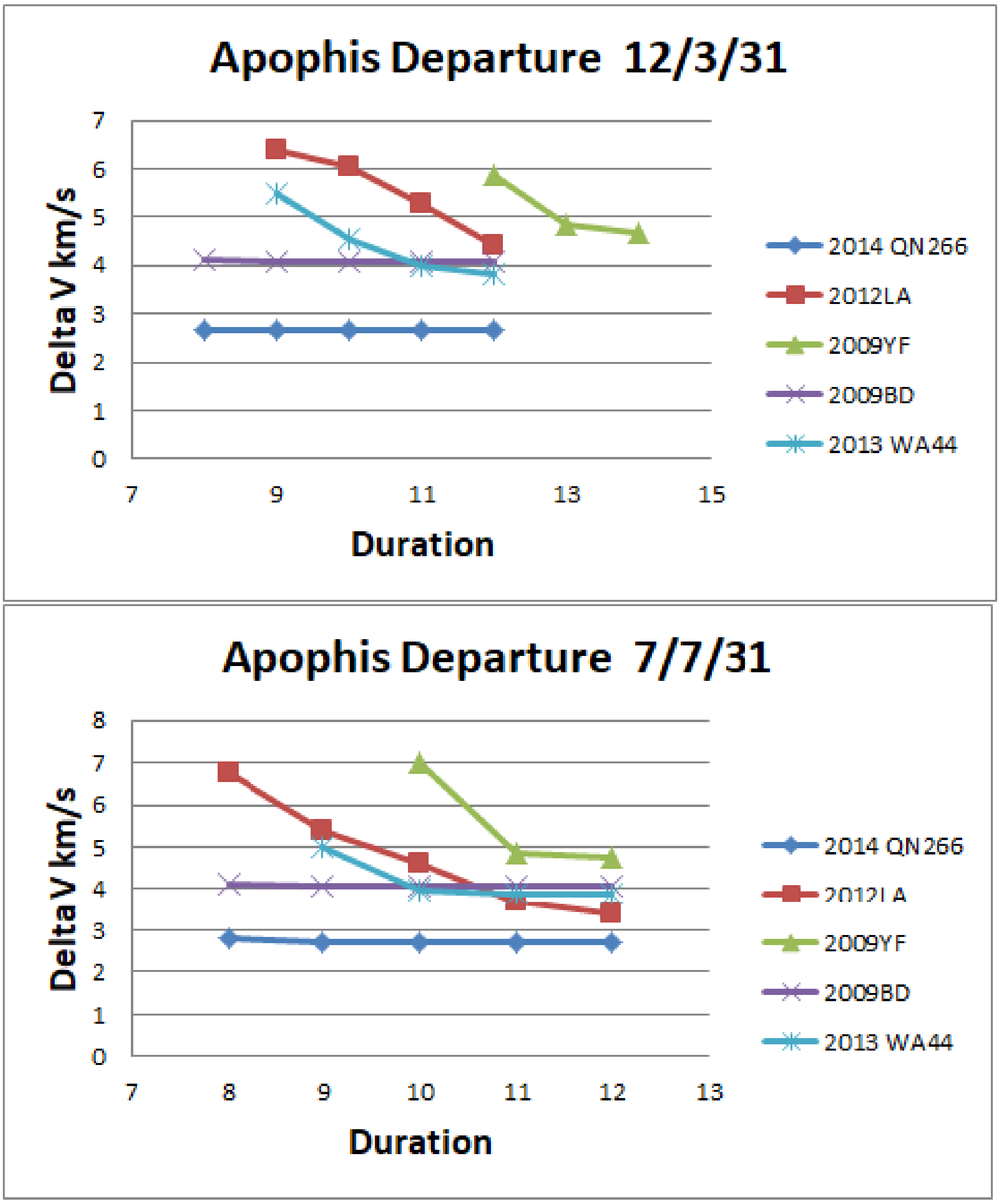


Figure 5.7: $\Delta V$ consumption respect to duration time for the sequence Apophis - Asteroid X

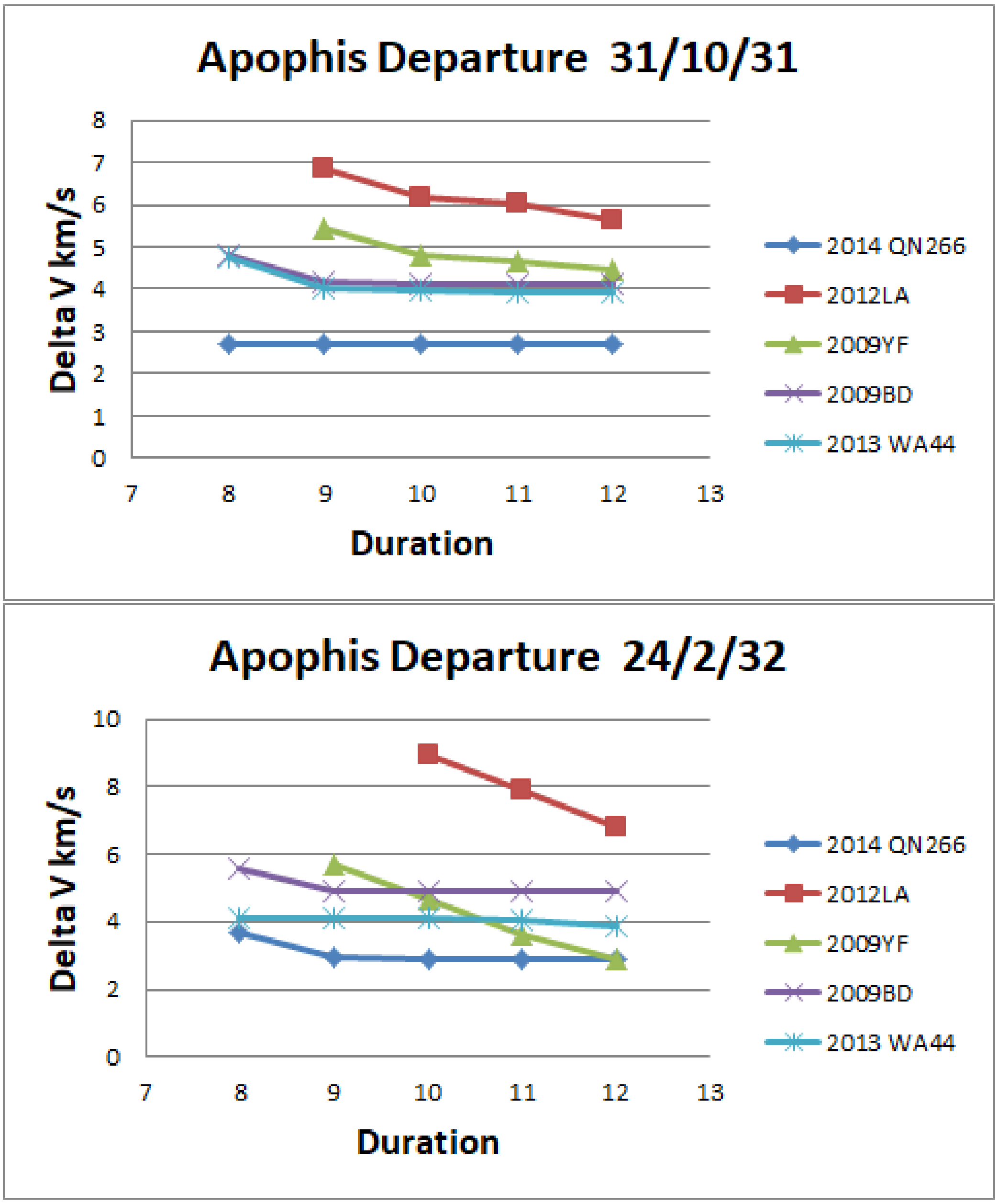


Figure 5.8: $\Delta V$ consumption respect to duration time for the sequence Apophis - Asteroid X

To have a confirm of the previous studies, the total trajectory sequence was evaluated, changing the last asteroid, with different departure dates from Earth; as we can see in figures 5.9 and 5.10 the lowest $\Delta V$ consumption occurs with 2014 QN266 as final Asteroid.

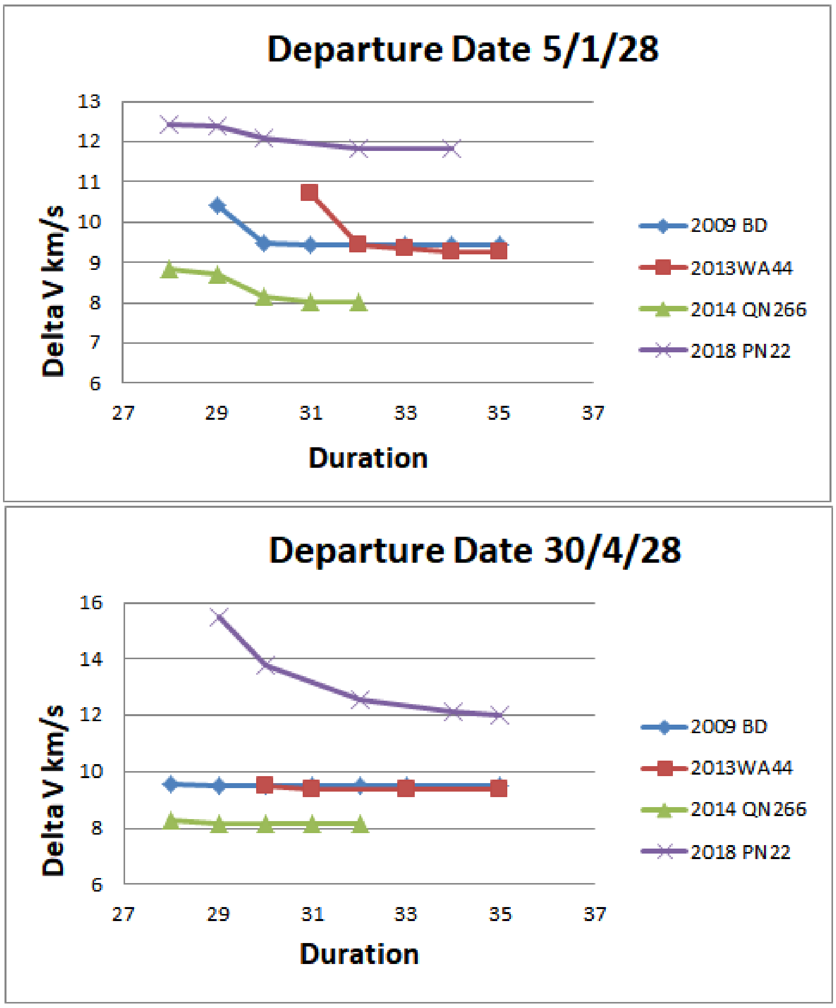


Figure 5.9: DeltaV consumption respect to duration time (in this graph 1 unit=2 months), the different color lines represent different asteroids in the sequence Earth - 2012 LA - Apophis - X .

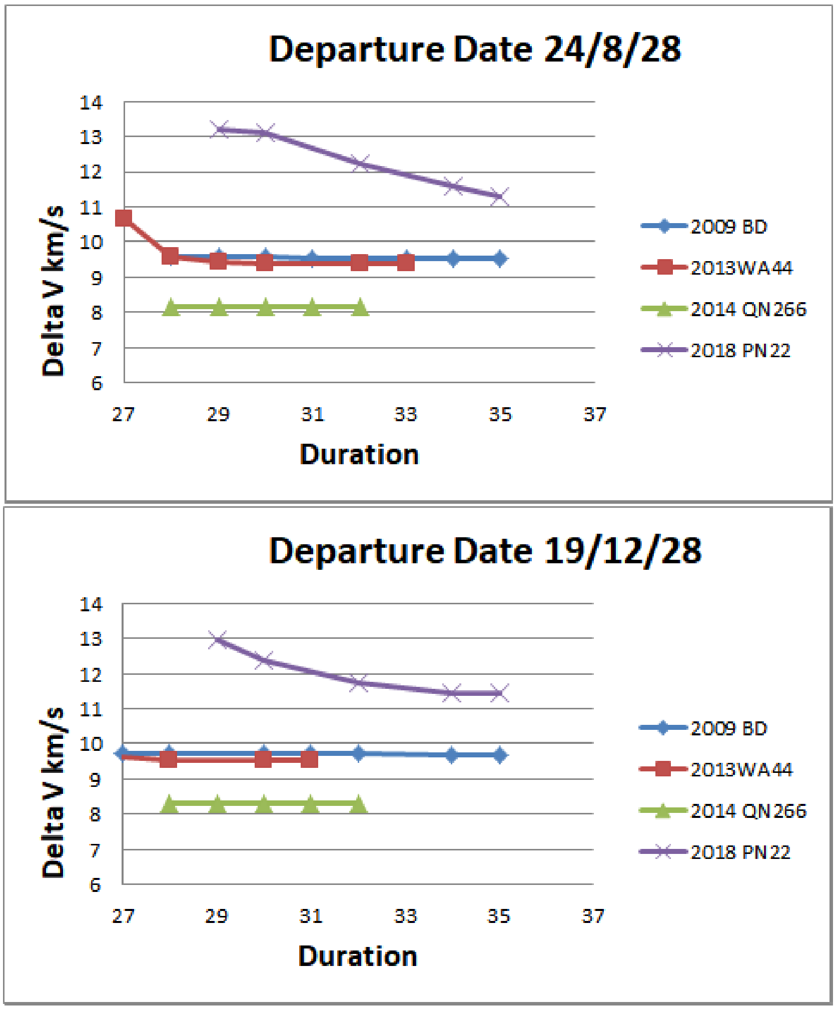


Figure 5.10: DeltaV consumption respect to duration time for the sequence Earth - 2012 LA - Apophis - X .

## 5.3 Final Trajectory Analysis

In this section we analyse the final selected trajectory: Earth - 2012 LA - Apophis - 2014 QN266 to choose the best solutions. Again were evaluated different departure dates from Earth, with an interval of two months from each other, with different journey durations and we compared them. We noticed that the spacecraft can reach Apophis optimally in two particularly dates, one earlier and one later.

### 5.3.1 Early Apophis Arrive

In this solutions the spacecraft reaches Apophis in the middle of 2031. The obtained solutions are summarized in the figure 5.11.

Analysing the graph we selected four possible trajectory solutions.

| Solution | Earth Departure | 2014 QN266 Arrival | $\Delta V_{tot}$ [km/s] |
|---|---|---|---|
| 1A | 27/06/28 | 22/4/32 | 8.962 |
| 1B | 27/06/28 | 6/4/33 | 8.341 |
| 1C | 19/12/28 | 14/10/32 | 8.462 |
| 1D | 19/12/28 | 28/9/33 | 8.333 |

Table 5.11: Apophis Early Arrival solutions

For each solution are represented the spacecraft trajectory, the Switching Function, the Thrust, the Available Power and the distance from the Sun among the time.

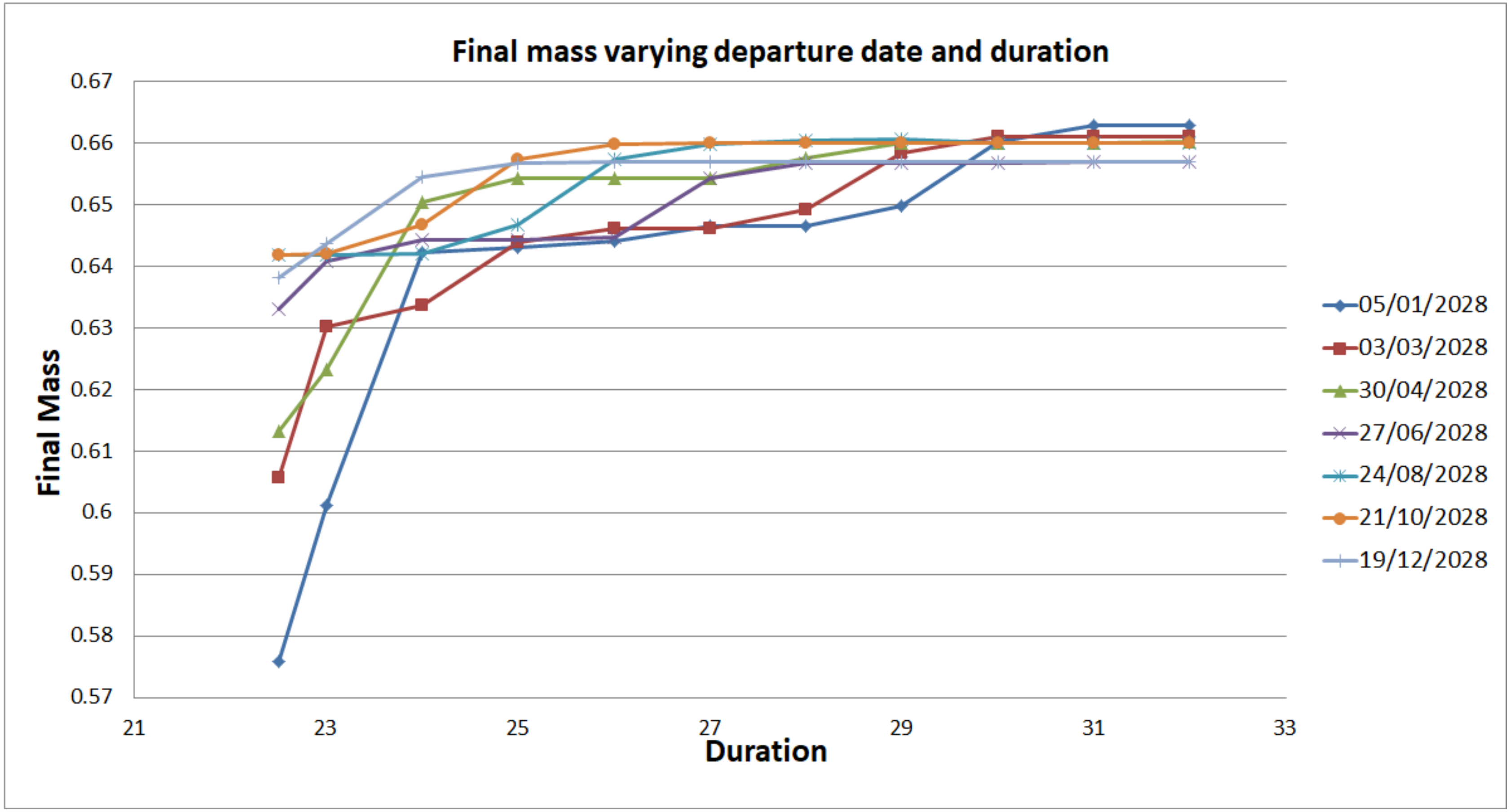


Figure 5.11: Final Spacecraft mass respect to duration time,initial mass 0.85, (in this graph 1 unit=2 months), the different color lines represent different Earth departure Date in the sequence Earth - 2012 LA - Apophis - 2014 QN266 with Apophis arrival in middle 2031.

### Solution 1A

| Earth Dep. | 2012LA Arr. | Apophis Arr. | 2014QN266 Arr. | $\Delta V_{tot}$ [km/s] | Mass [kg] |
|---|---|---|---|---|---|
| 27/06/28 | 24/7/29 | 18/4/31 | 22/4/32 | 8.962 | 644 |

Table 5.12: Solution 1A

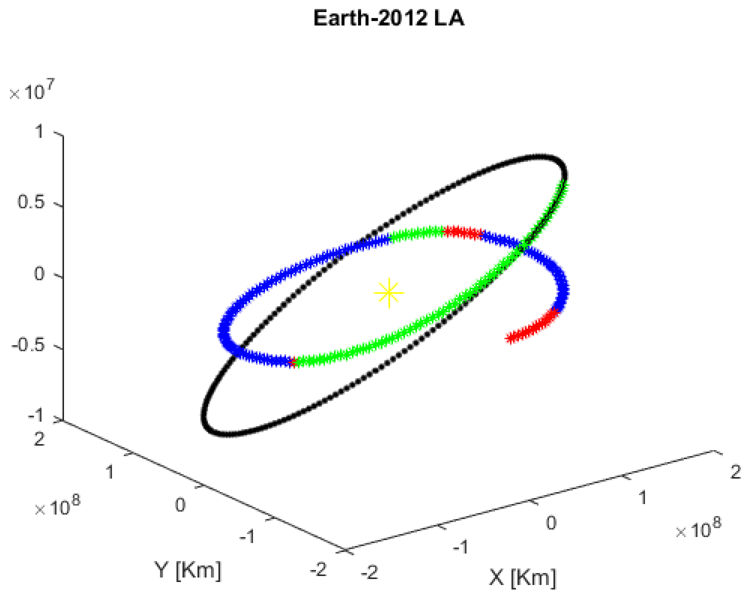


Figure 5.12: Spacecraft trajectory from Earth to 2012 LA.The blue points represent trajectory with zero thrust, green points with thrust > 0, red points thrust < 0,black points represent 2012 LA trajectory.

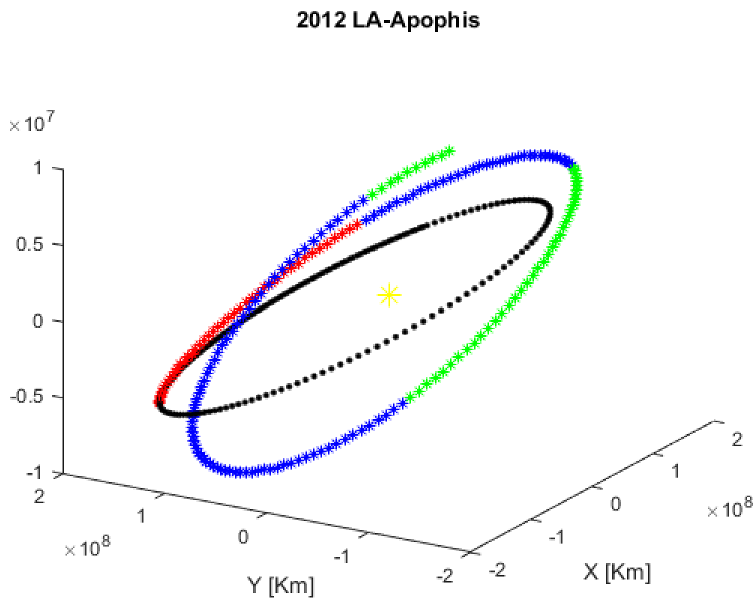


Figure 5.13: Spacecraft trajectory from 2012 LA to Apophis .Black points represent Apophis trajectory.

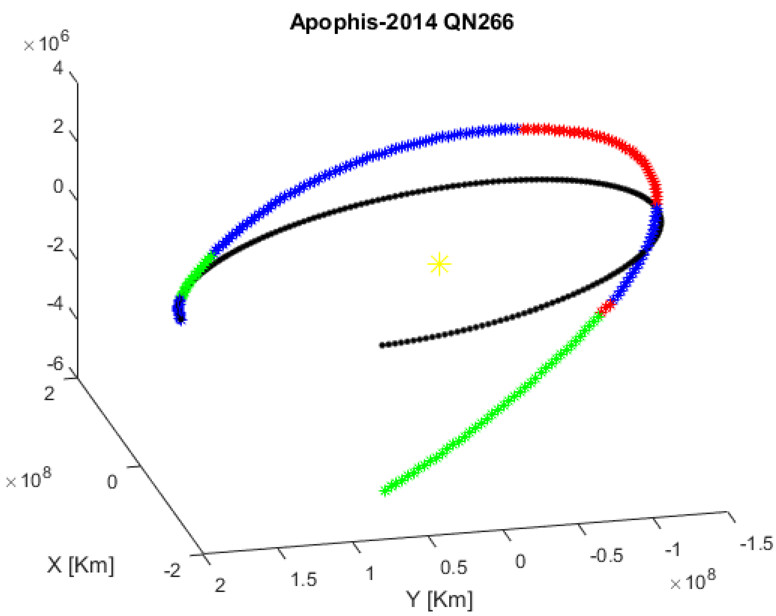


Figure 5.14: Spacecraft trajectory from Apophis to 2014 QN266A.Black points represent 2014 QN266 trajectory.

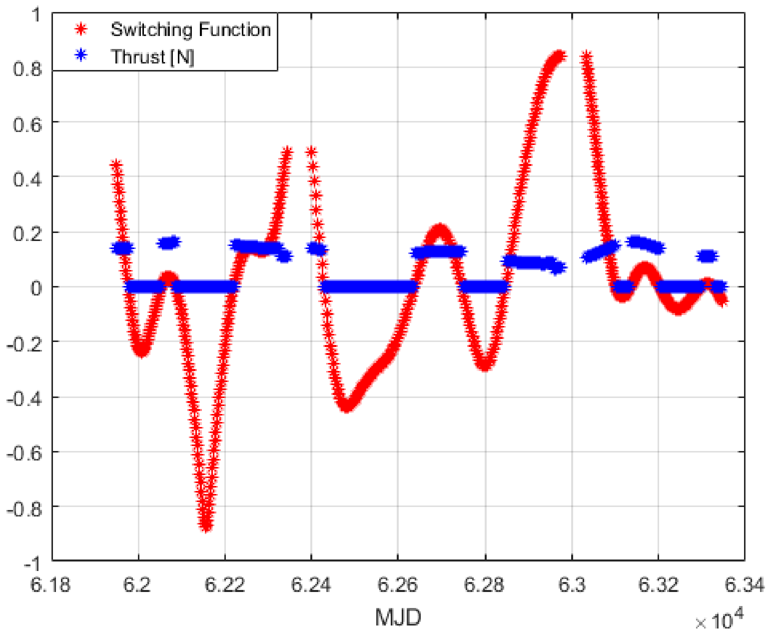


Figure 5.15: Switching Function and Thrust

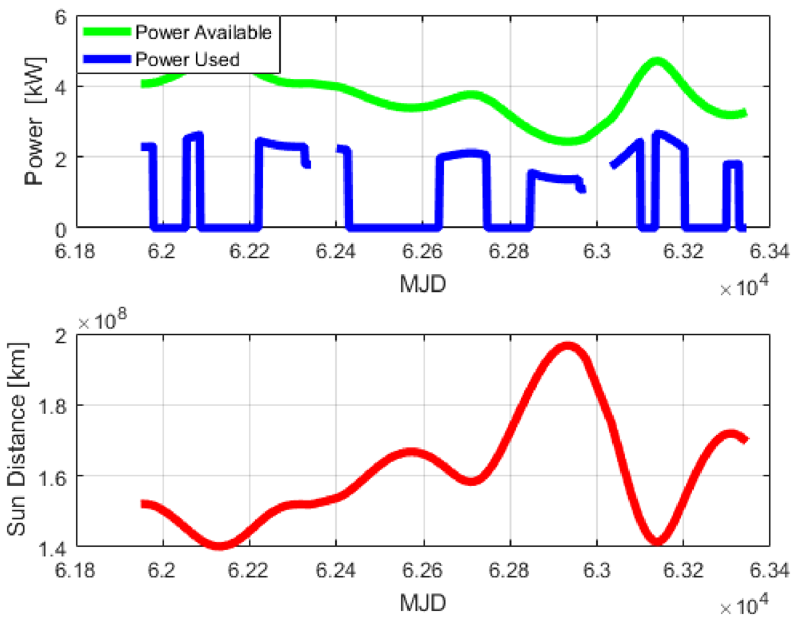


Figure 5.16: Power available and distance from the sun during the journey.

### Solution 1B

| Earth Dep. | 2012LA Arr. | Apophis Arr. | 2014QN266 Arr. | $\Delta V_{tot}$ [km/s] | Mass [kg] |
|---|---|---|---|---|---|
| 27/06/28 | 5/10/29 | 16/7/31 | 6/4/33 | 8.341 | 657 |

Table 5.13: Solution 1B

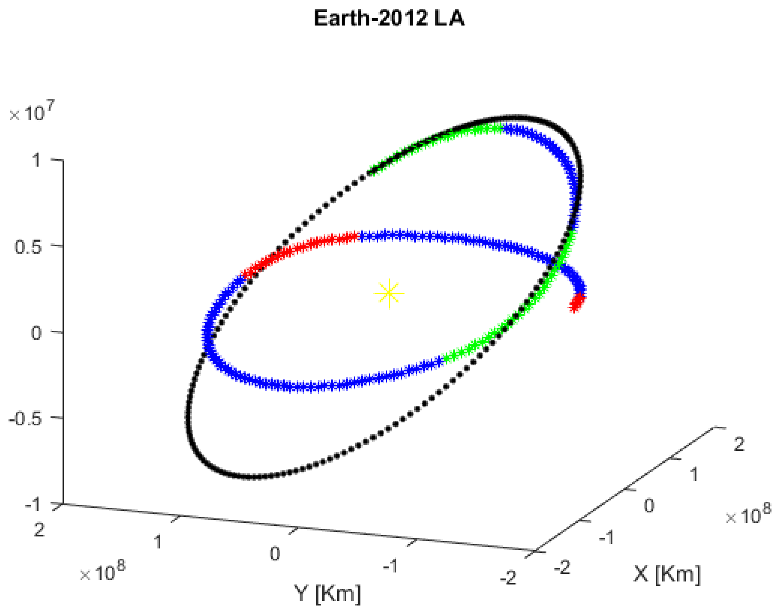


Figure 5.17: Spacecraft trajectory from Earth to 2012 LA.Black points represent 2012 LA trajectory.

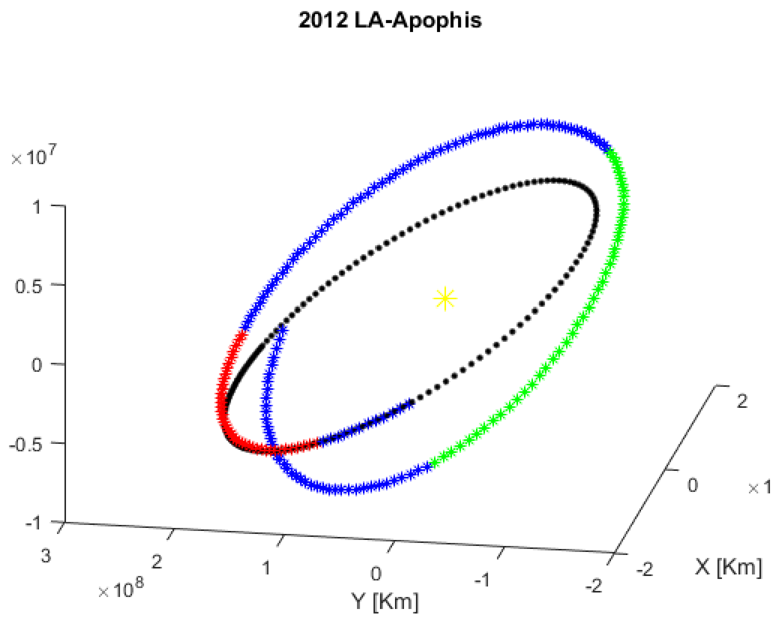


Figure 5.18: Spacecraft trajectory from 2012 LA to Apophis .Black points represent Apophis trajectory.

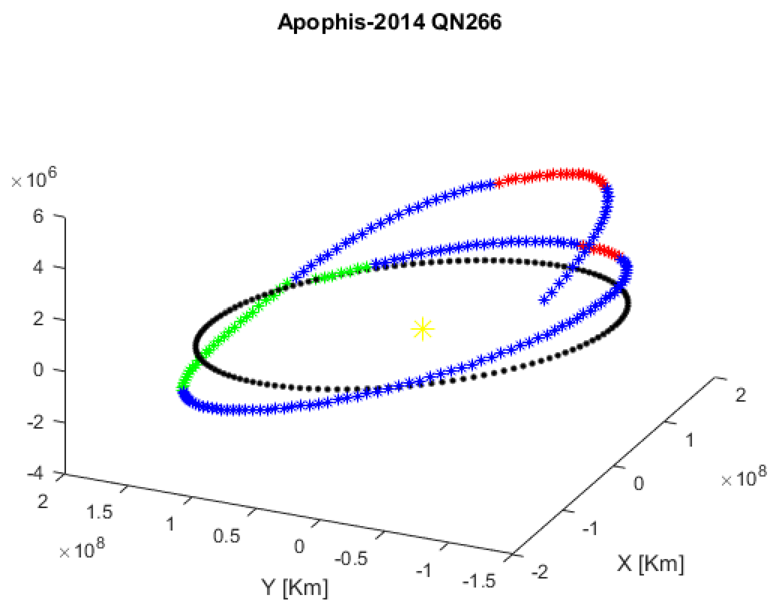


Figure 5.19: Spacecraft trajectory from Apophis to 2014 QN266A.Black points represent 2014 QN266 trajectory.

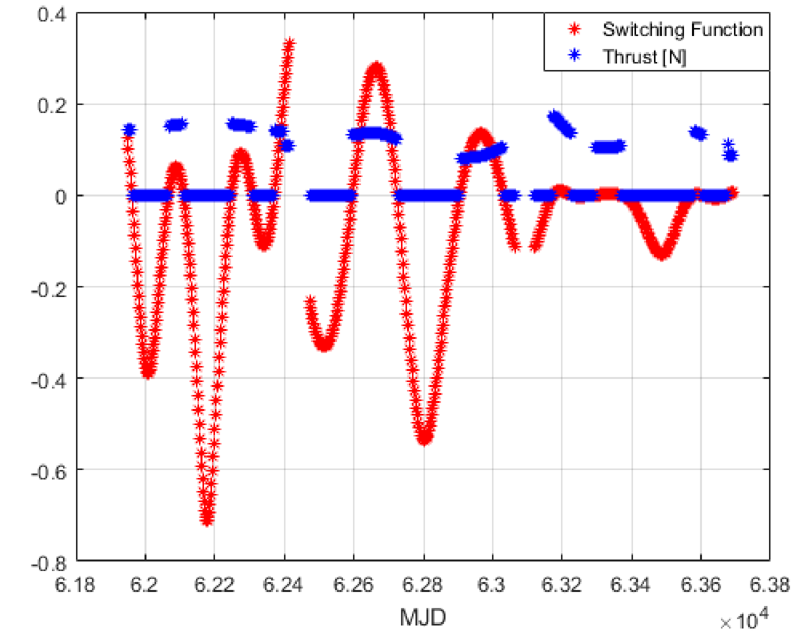


Figure 5.20: Switching Function and Thrust

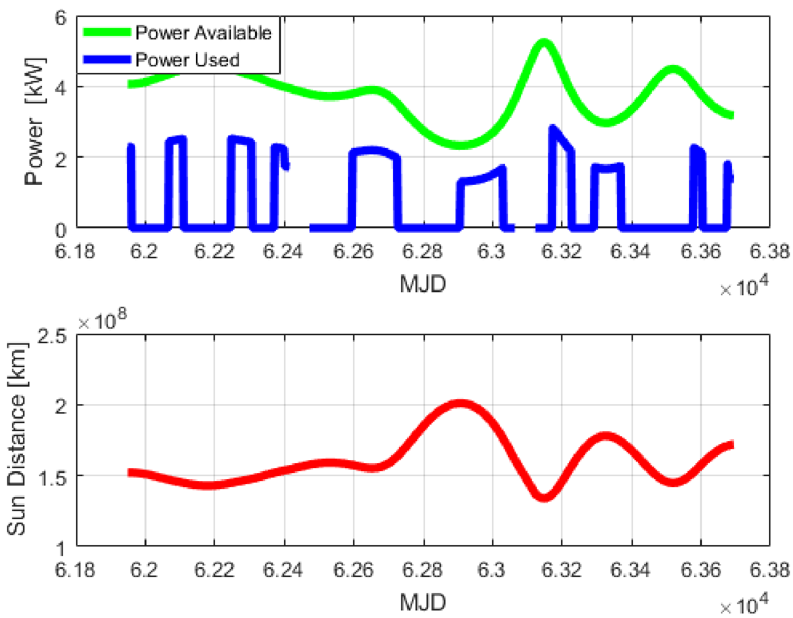


Figure 5.21: Power available and distance from the sun during the journey.

### Solution 1C

| Earth Dep. | 2012LA Arr. | Apophis Arr. | 2014QN266 Arr. | $\Delta V_{tot}$ [km/s] | Mass [kg] |
|---|---|---|---|---|---|
| 19/12/28 | 7/02/30 | 16/6/31 | 14/10/32 | 8.462 | 654 |

Table 5.14: Solution 1C

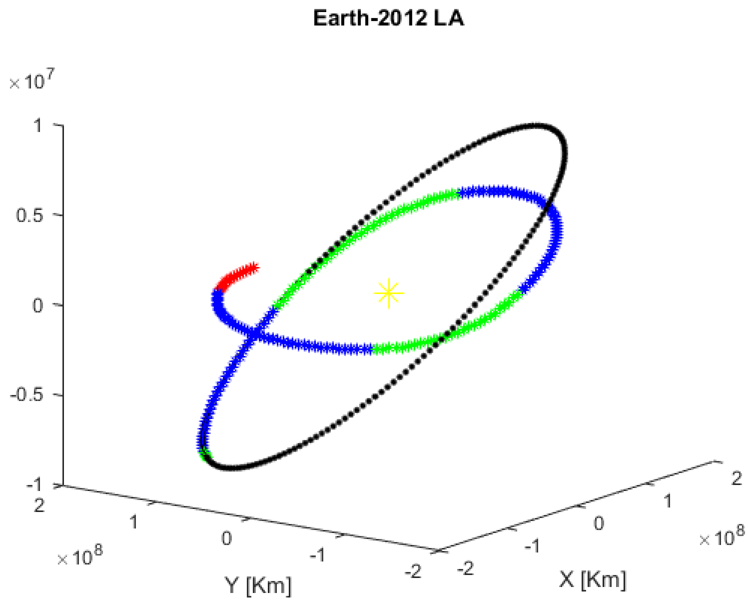


Figure 5.22: Spacecraft trajectory from Earth to 2012 LA.Black points represent 2012 LA trajectory.

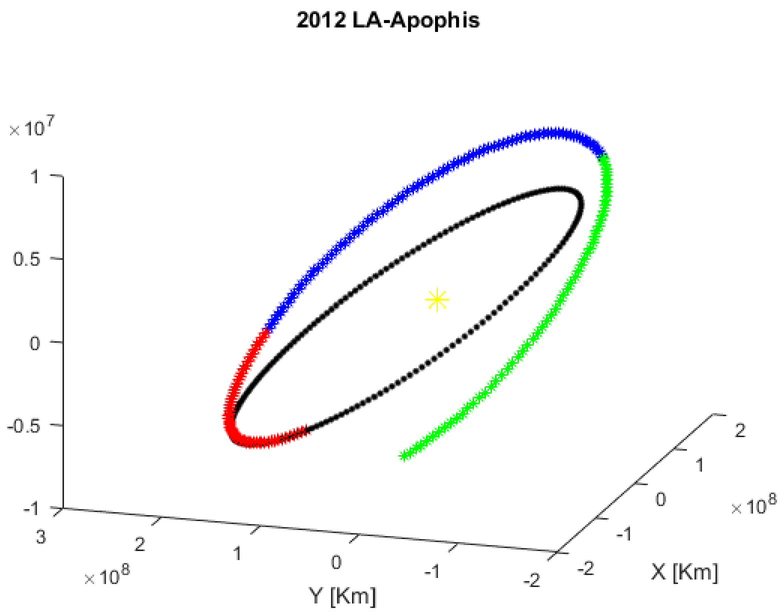


Figure 5.23: Spacecraft trajectory from 2012 LA to Apophis .Black points represent Apophis trajectory.

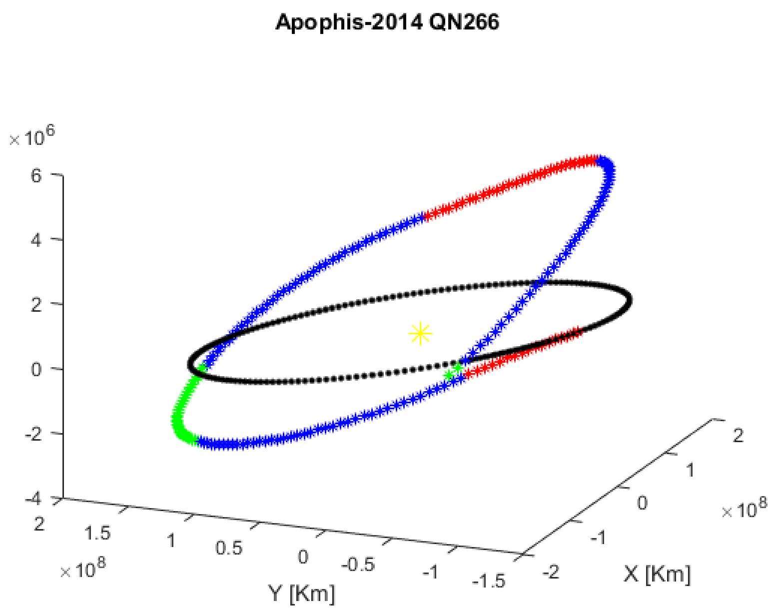


Figure 5.24: Spacecraft trajectory from Apophis to 2014 QN266A.Black points represent 2014 QN266 trajectory.

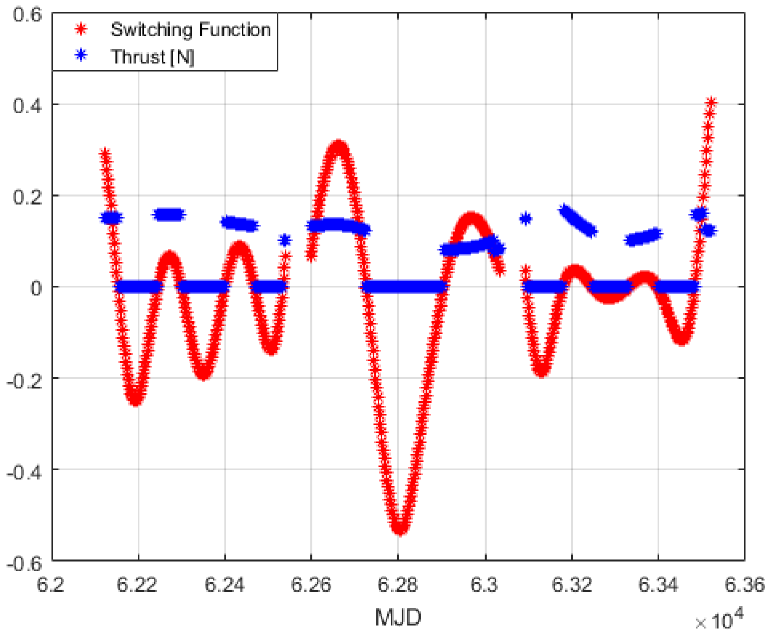


Figure 5.25: Switching Function and Thrust

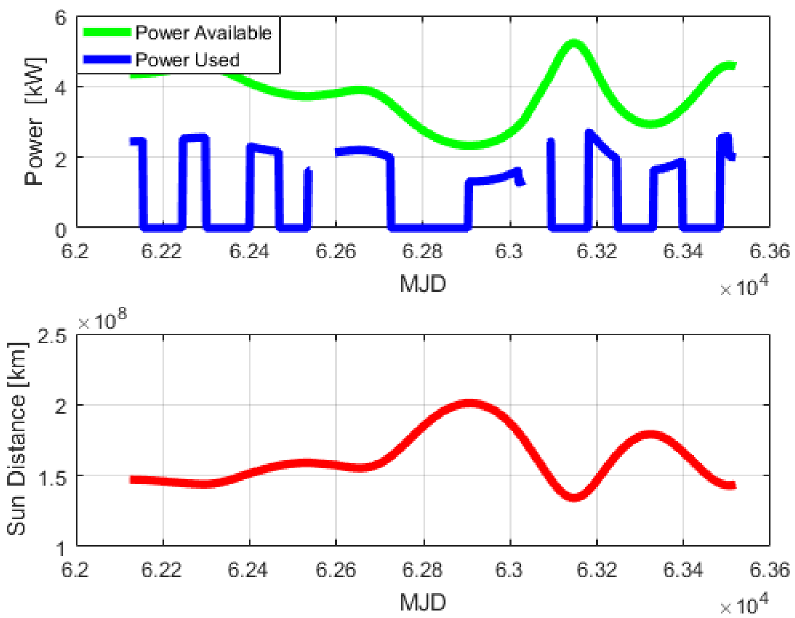


Figure 5.26: Power available and distance from the sun during the journey.

### Solution 1D

| Earth Dep. | 2012LA Arr. | Apophis Arr. | 2014QN266 Arr. | $\Delta V_{tot}$ [km/s] | Mass [kg] |
|---|---|---|---|---|---|
| 19/12/28 | 7/02/30 | 21/7/31 | 28/9/33 | 8.333 | 657 |

Table 5.15: Solution 1D

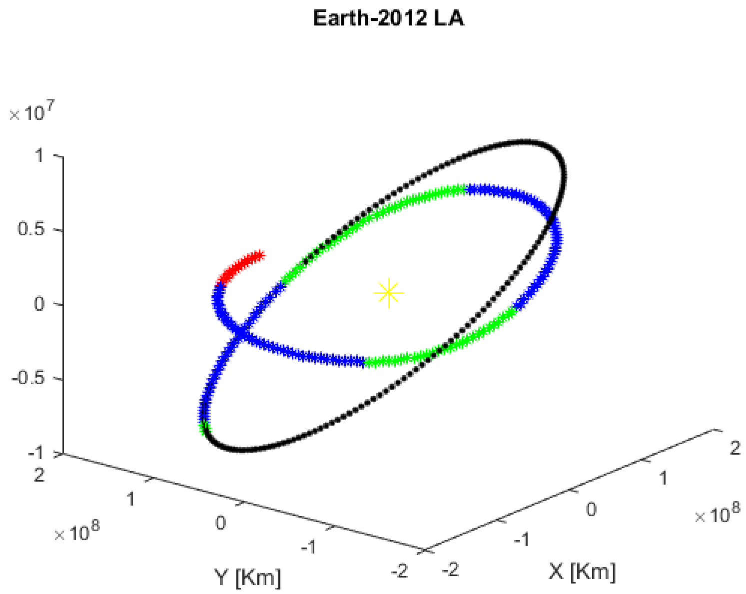


Figure 5.27: Spacecraft trajectory from Earth to 2012 LA.Black points represent 2012 LA trajectory.

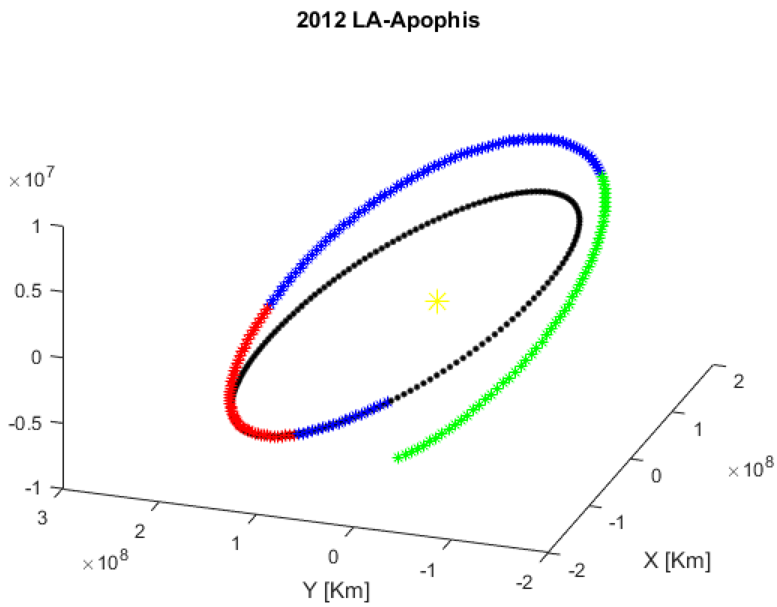


Figure 5.28: Spacecraft trajectory from 2012 LA to Apophis .Black points represent Apophis trajectory.

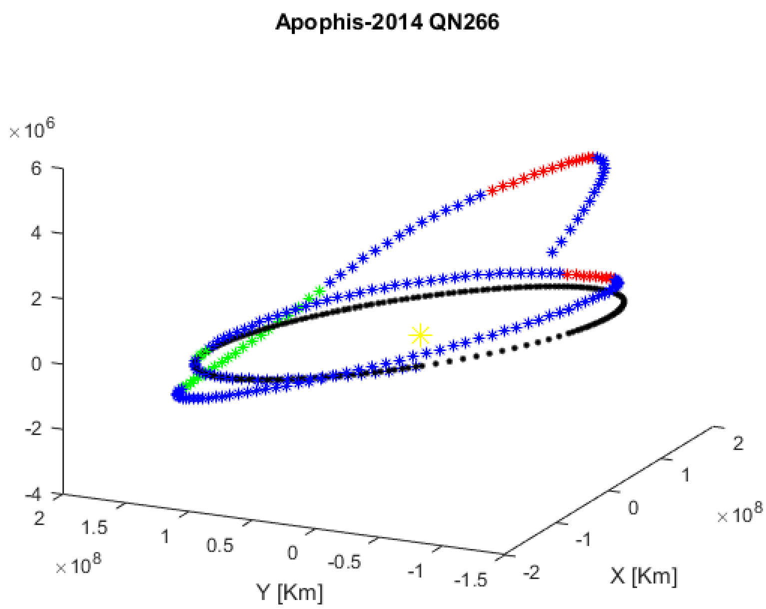


Figure 5.29: Spacecraft trajectory from Apophis to 2014 QN266A.Black points represent 2014 QN266 trajectory.

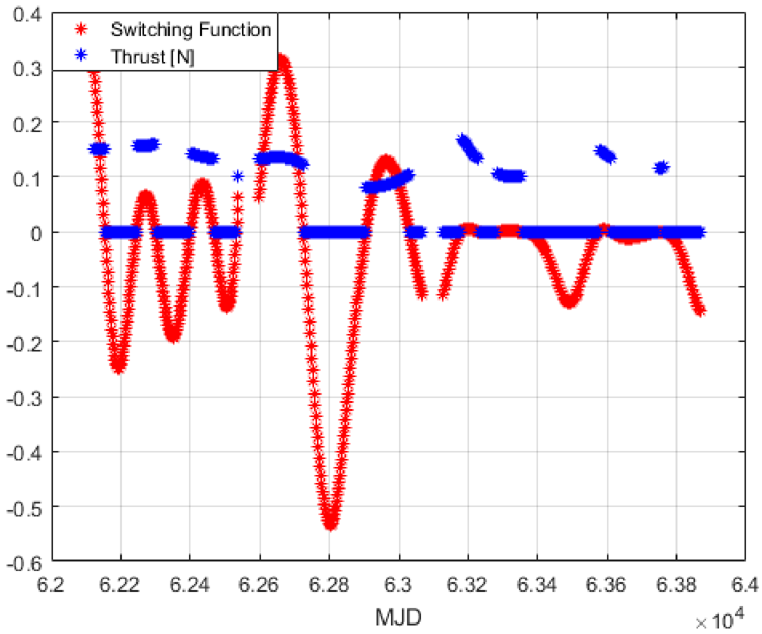


Figure 5.30: Switching Function and Thrust

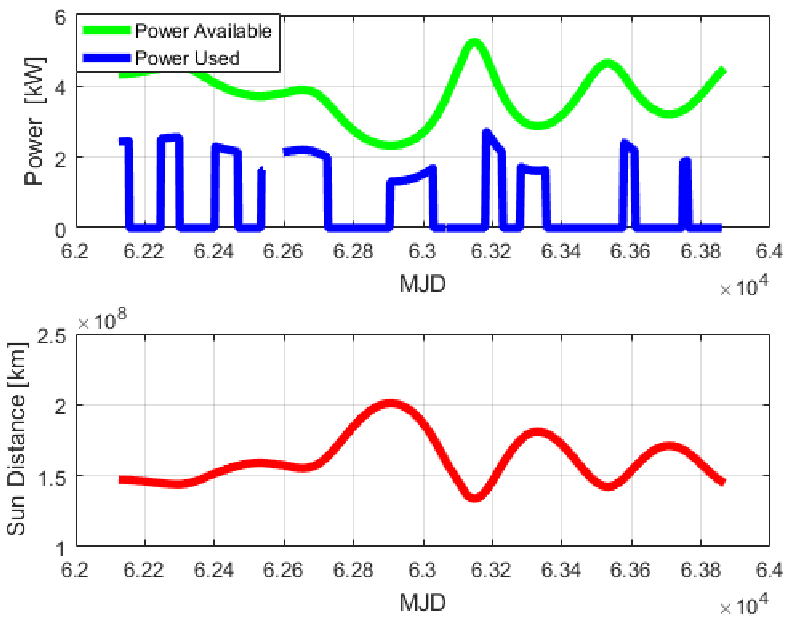


Figure 5.31: Power available and distance from the sun during the journey.

### 5.3.2 Late Apophis Arrive

In this solutions the spacecraft reaches Apophis at the end of 2031 or at the beginning of 2032. The obtained solutions are summarized in the figure 5.32.

Analysing the graph we selected again four possible trajectory solutions.

| Solution | Earth Departure | 2014 QN266 Arrival | $\Delta V_{tot}$ [km/s] |
|---|---|---|---|
| 2A | 27/06/28 | 14/10/32 | 8.311 |
| 2B | 27/06/28 | 6/4/33 | 8.193 |
| 2C | 19/12/28 | 6/4/33 | 8.346 |
| 2D | 19/12/28 | 28/9/33 | 7.959 |

Table 5.16: Apophis Late Arrive solutions

For each solution are represented the spacecraft trajectory, the Switching Function, the Thrust, the Available Power and the distance from the Sun among the time.

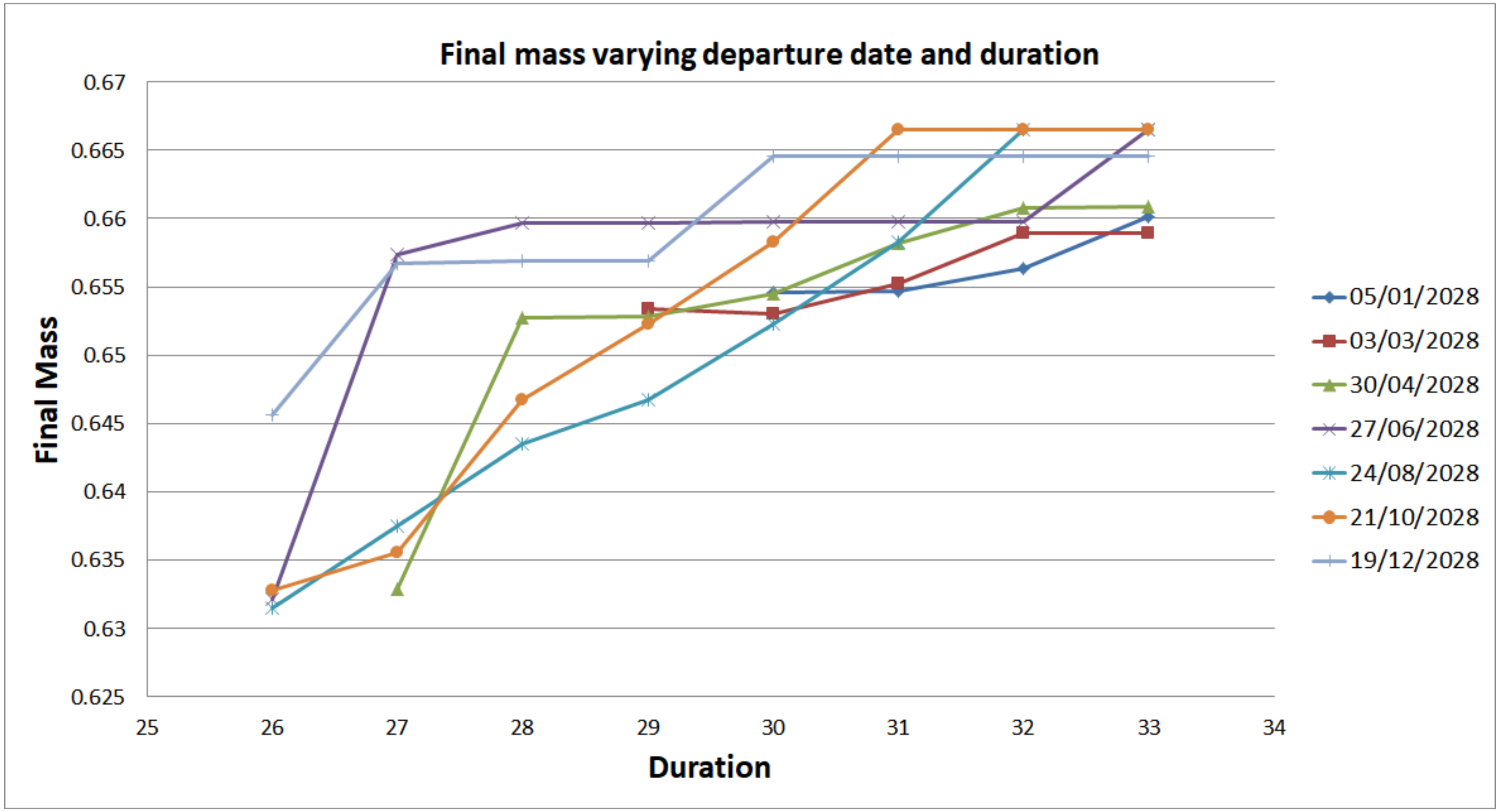


Figure 5.32: Final Spacecraft mass respect to duration time,initial mass 0.85, (in this graph 1 unit=2 months), the different color lines represent different Earth departure Date in the sequence Earth - 2012 LA - Apophis - 2014 QN266 with Apophis arrival in the beginning of 2032.

### Solution 2A

| Earth Dep. | 2012LA Arr. | Apophis Arr. | 2014QN266 Arr. | $\Delta V_{tot}$ [km/s] | Mass [kg] |
|---|---|---|---|---|---|
| 27/06/28 | 28/12/29 | 14/9/31 | 14/10/32 | 8.311 | 657 |

Table 5.17: Solution 2A

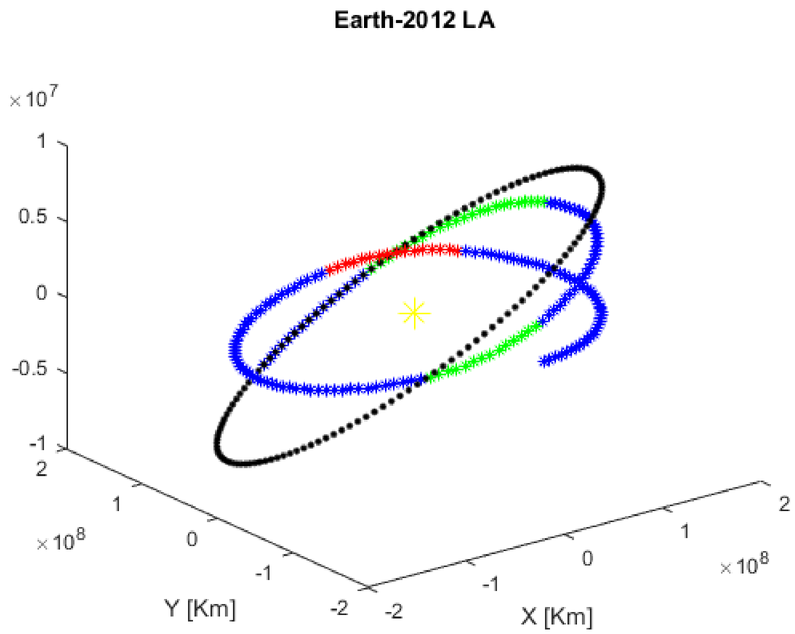


Figure 5.33: Spacecraft trajectory from Earth to 2012 LA.Black points represent 2012 LA trajectory.

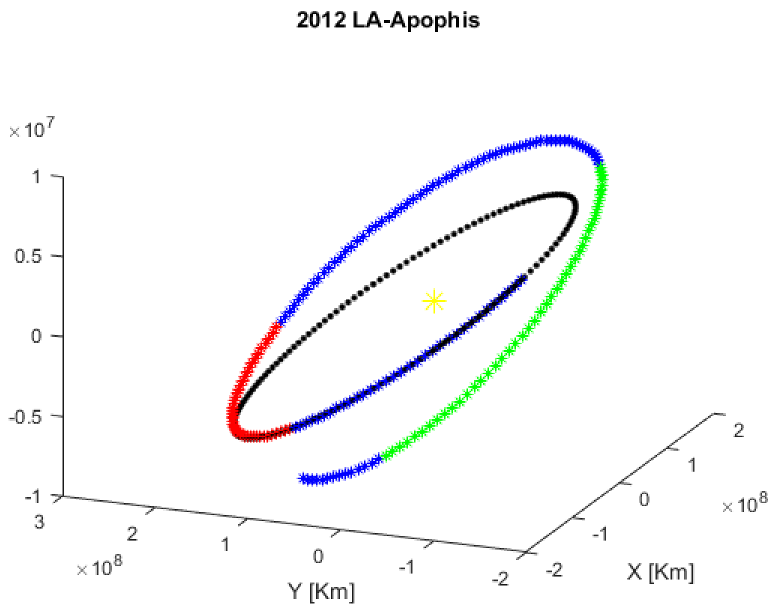


Figure 5.34: Spacecraft trajectory from 2012 LA to Apophis .Black points represent Apophis trajectory.

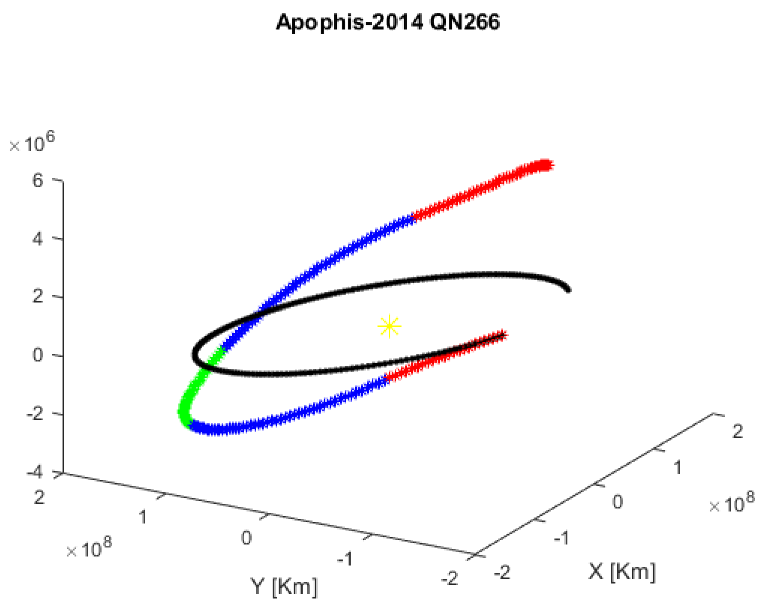


Figure 5.35: Spacecraft trajectory from Apophis to 2014 QN266A.Black points represent 2014 QN266 trajectory.

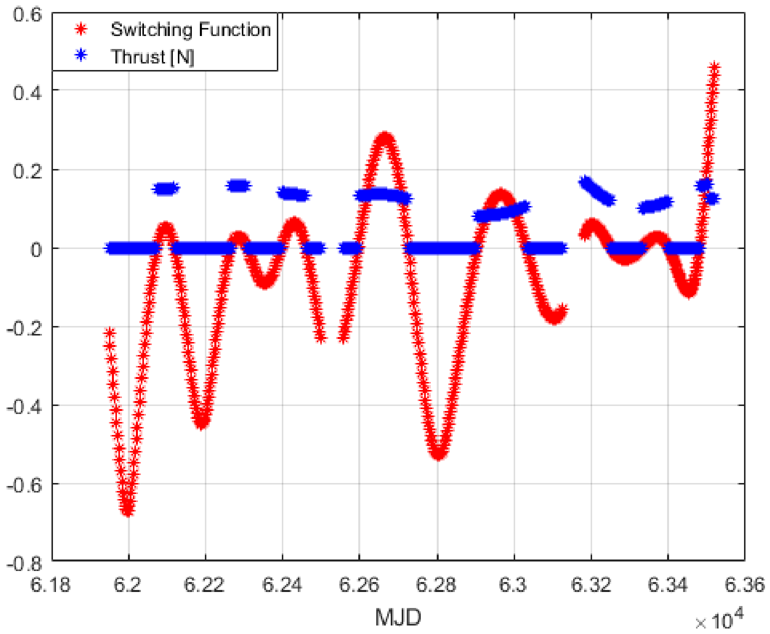


Figure 5.36: Switching Function and Thrust

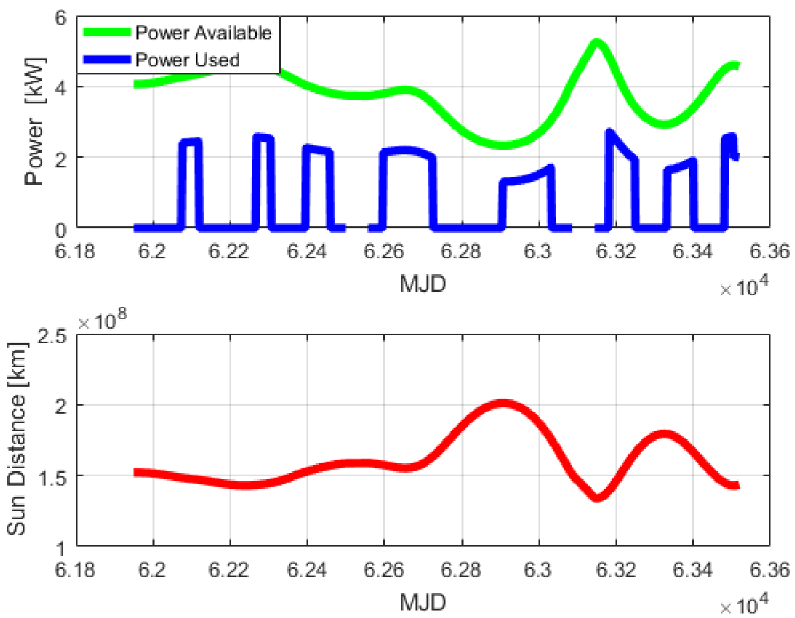


Figure 5.37: Power available and distance from the sun during the journey.

### Solution 2B

| Earth Dep. | 2012LA Arr. | Apophis Arr. | 2014QN266 Arr. | $\Delta V_{tot}$ [km/s] | Mass [kg] |
|---|---|---|---|---|---|
| 27/06/28 | 28/12/29 | 14/9/31 | 6/4/33 | 8.193 | 660 |

Table 5.18: Solution 2B

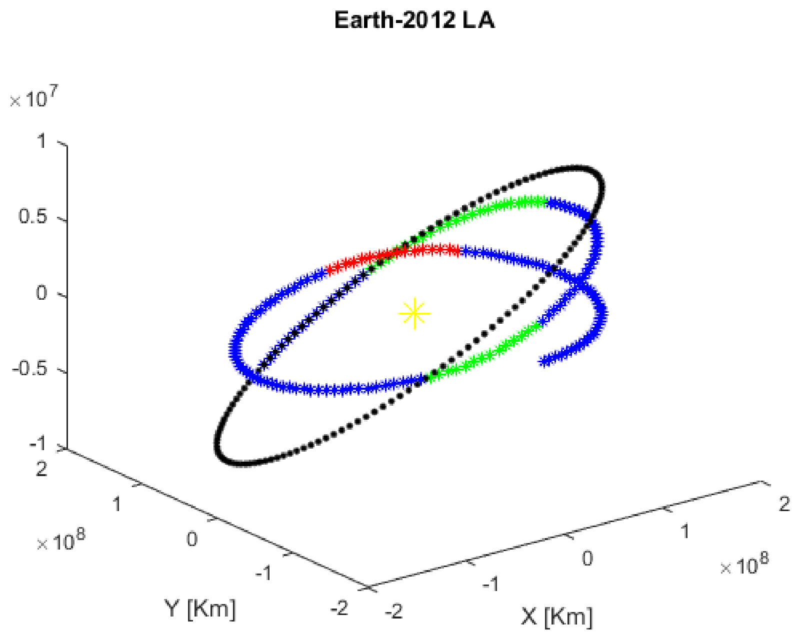


Figure 5.38: Spacecraft trajectory from Earth to 2012 LA.Black points represent 2012 LA trajectory.

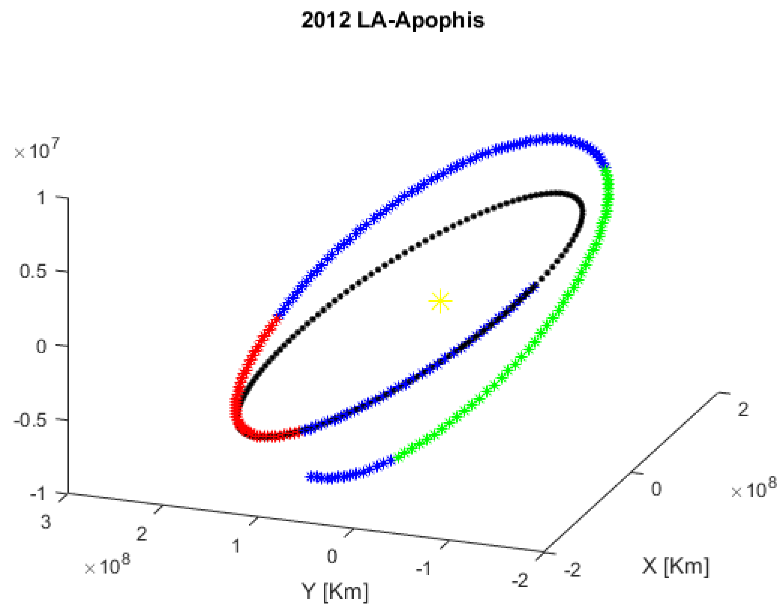


Figure 5.39: Spacecraft trajectory from 2012 LA to Apophis .Black points represent Apophis trajectory.

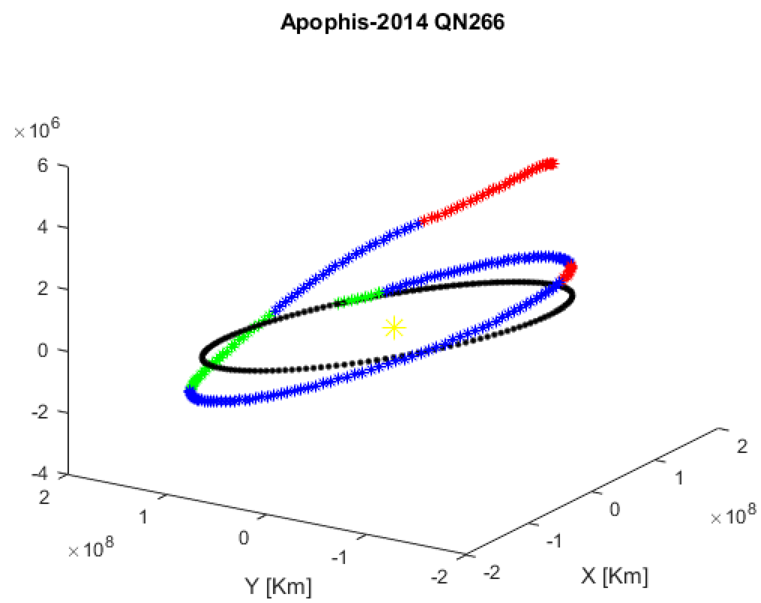


Figure 5.40: Spacecraft trajectory from Apophis to 2014 QN266A.Black points represent 2014 QN266 trajectory.

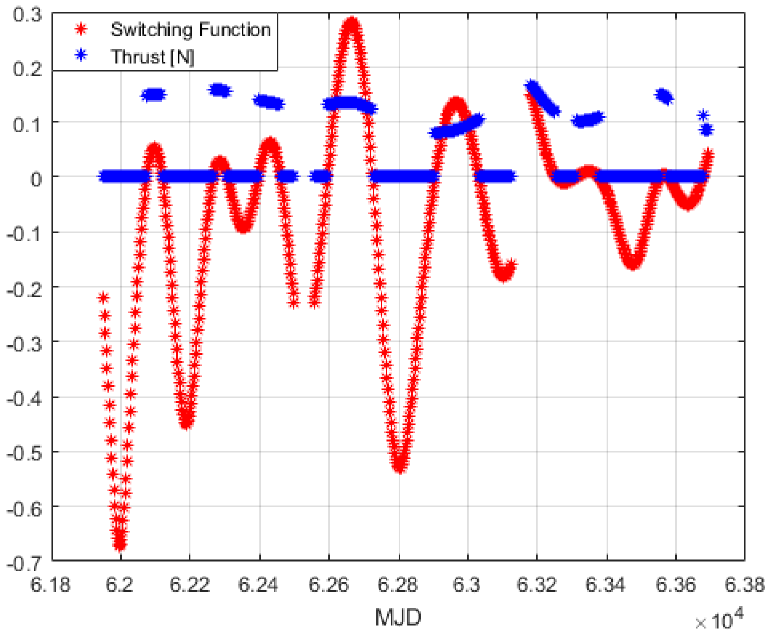


Figure 5.41: Switching Function and Thrust

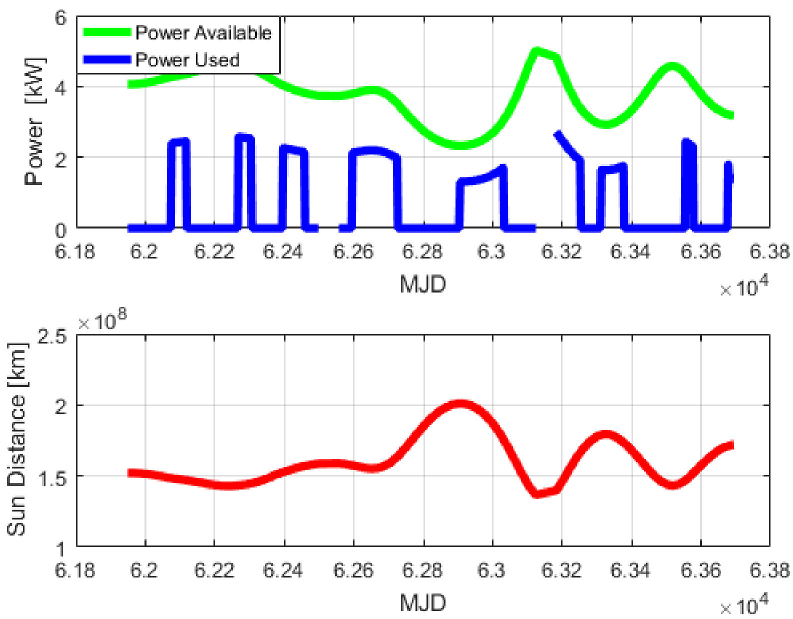


Figure 5.42: Power available and distance from the sun during the journey.

### Solution 2C

| Earth Dep. | 2012LA Arr. | Apophis Arr. | 2014QN266 Arr. | $\Delta V_{tot}$ [km/s] | Mass [kg] |
|---|---|---|---|---|---|
| 19/12/28 | 7/2/30 | 14/9/31 | 6/4/33 | 8.346 | 657 |

Table 5.19: Solution 2C

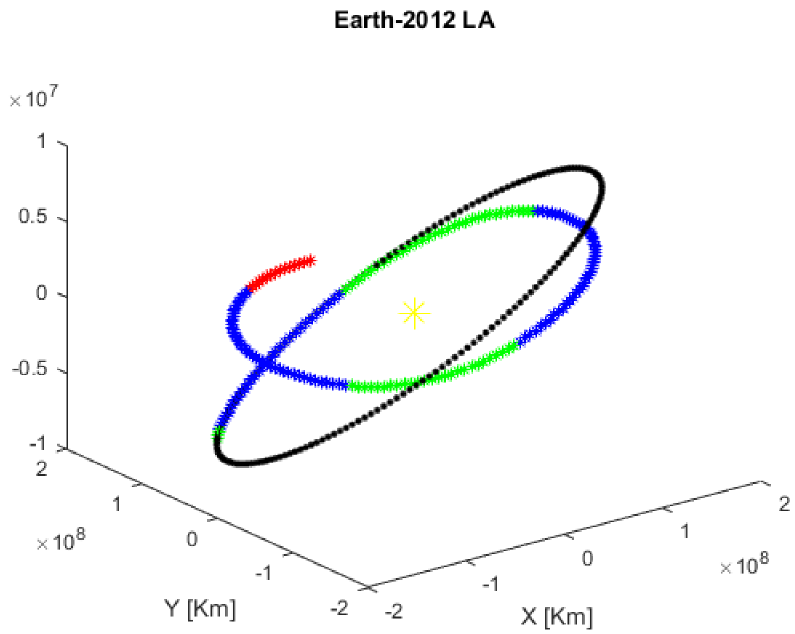


Figure 5.43: Spacecraft trajectory from Earth to 2012 LA.Black points represent 2012 LA trajectory.

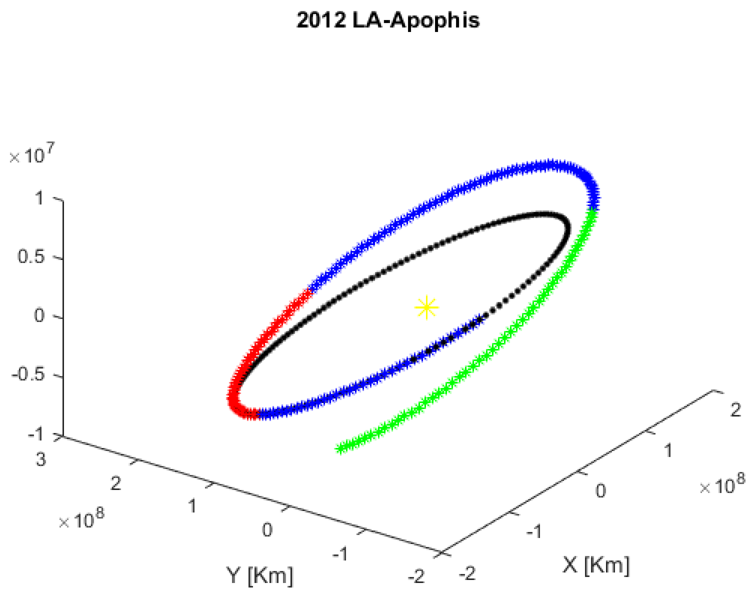


Figure 5.44: Spacecraft trajectory from 2012 LA to Apophis .Black points represent Apophis trajectory.

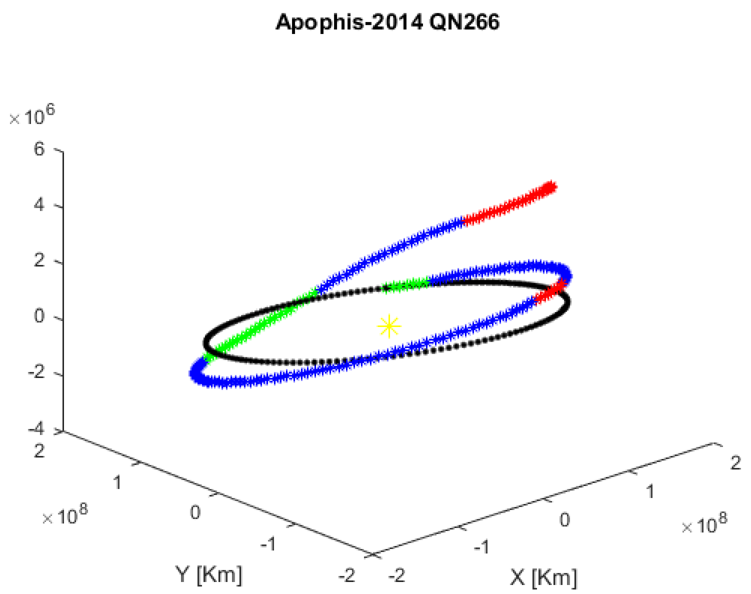


Figure 5.45: Spacecraft trajectory from Apophis to 2014 QN266A.Black points represent 2014 QN266 trajectory.

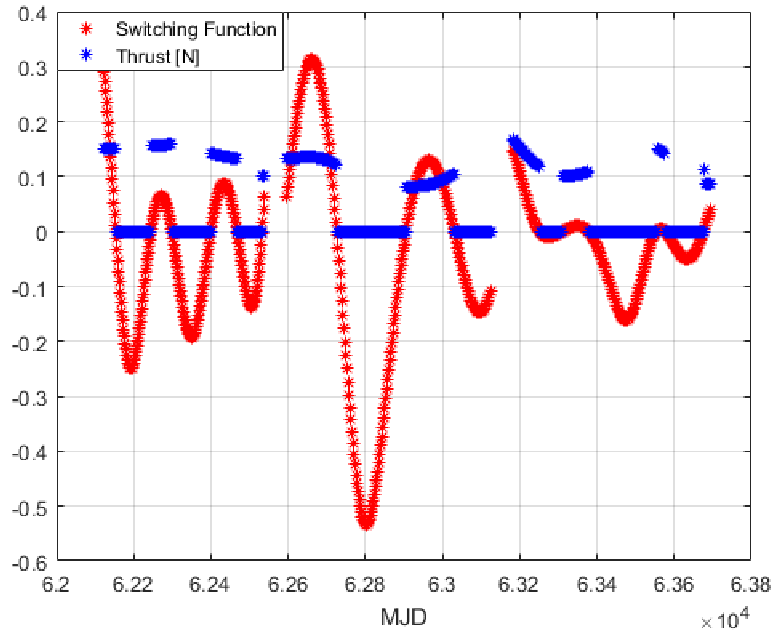


Figure 5.46: Switching Function and Thrust

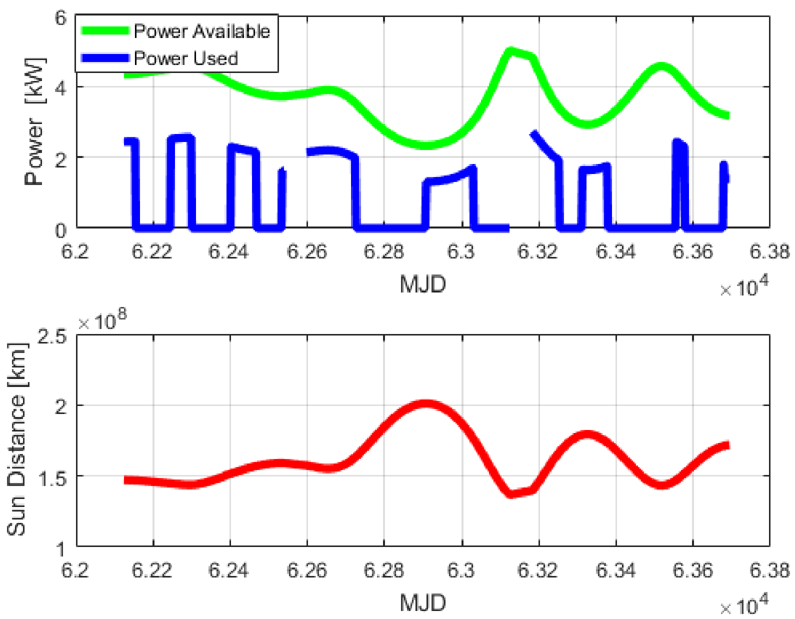


Figure 5.47: Power available and distance from the sun during the journey.

### Solution 2D

| Earth Dep. | 2012LA Arr. | Apophis Arr. | 2014QN266 Arr. | $\Delta V_{tot}$ [km/s] | Mass [kg] |
|---|---|---|---|---|---|
| 19/12/28 | 30/3/30 | 20/4/32 | 28/9/33 | 7.959 | 665 |

Table 5.20: Solution 2D

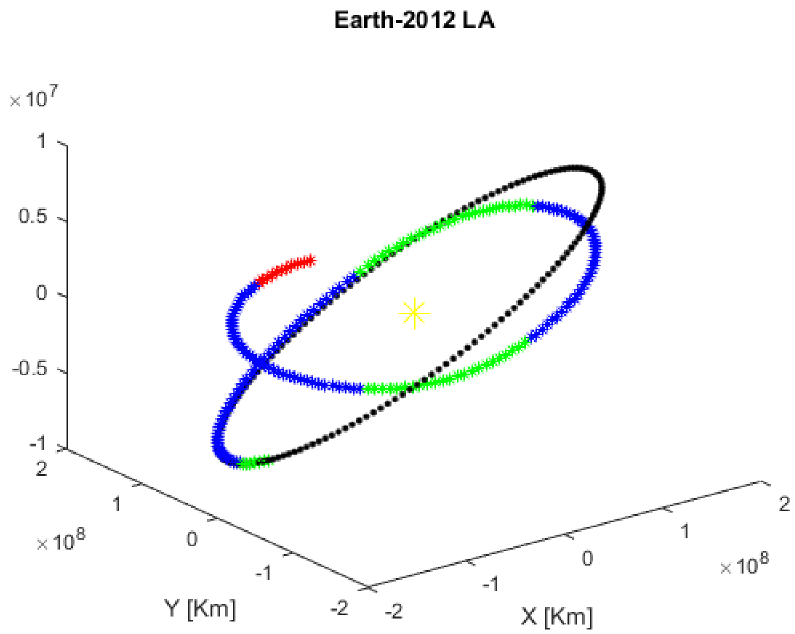


Figure 5.48: Spacecraft trajectory from Earth to 2012 LA. Black points represent 2012 LA trajectory.

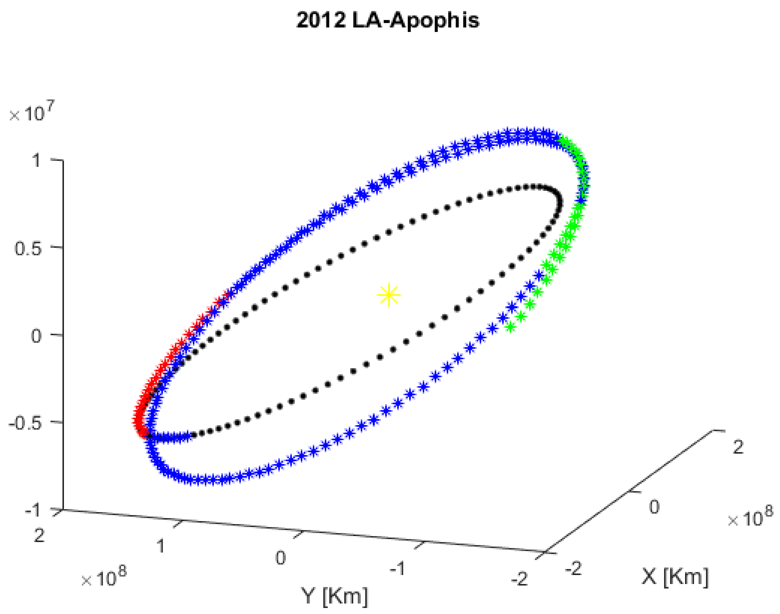


Figure 5.49: Spacecraft trajectory from 2012 LA to Apophis. Black points represent Apophis trajectory.

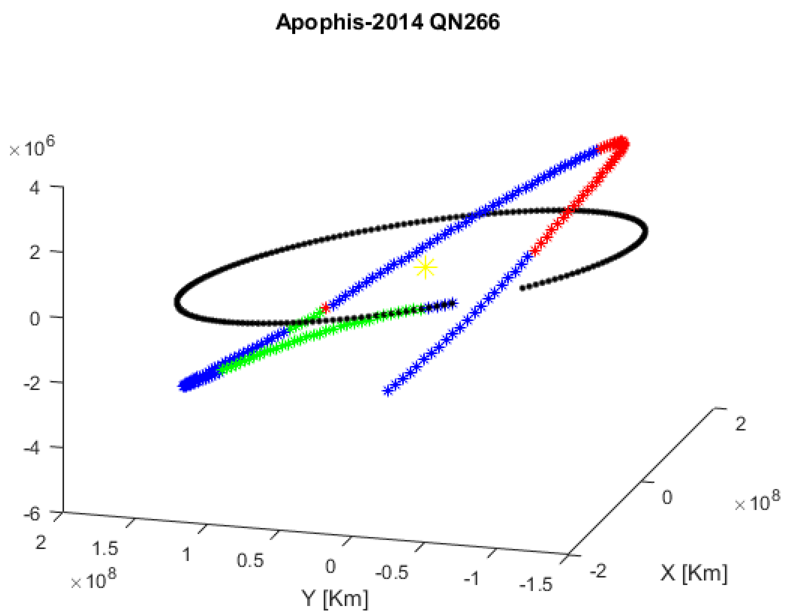


Figure 5.50: Spacecraft trajectory from Apophis to 2014 QN266A. Black points represent 2014 QN266 trajectory.

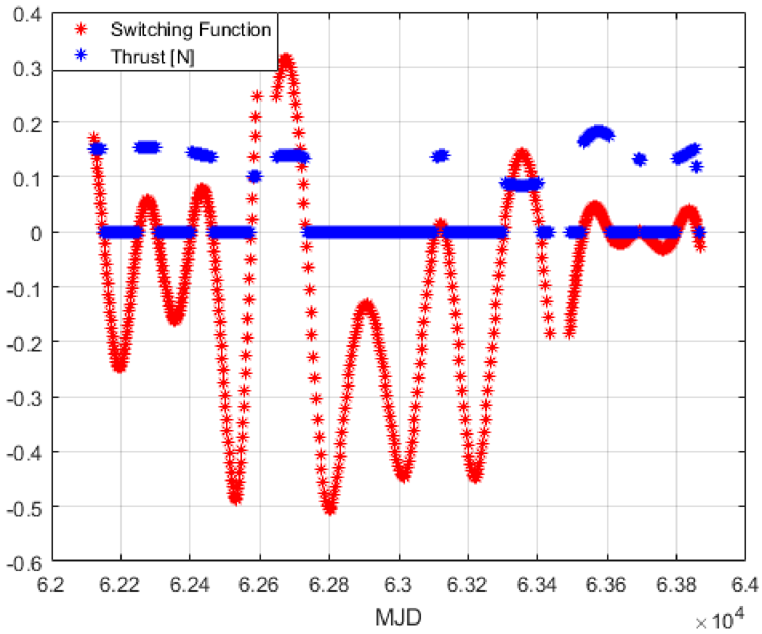


Figure 5.51: Switching Function and Thrust

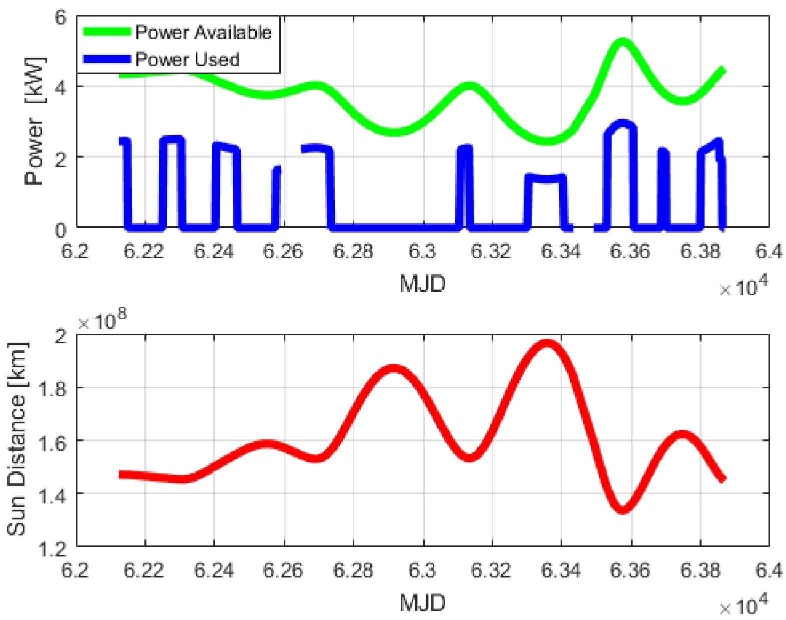


Figure 5.52: Power available and distance from the sun during the journey.

# Chapter 6

# Conclusions

In conclusion a preliminary method to select the best asteroids sequence was done in terms of fuel consumption and duration time, for a multiple asteroid rendezvous space mission. In particular, with the optimal control theory and indirect methods, were evaluated different trajectories solutions, with different asteroids for the NEST mission, with the constraints to have a departure date in 2028 and to not exceed a duration of five years. From the candidate asteroids the best trajectory sequence in terms of $\Delta V$ consumption was: Earth - 2012 LA - Apophis - 2014 QN 266. The obtained sequence was then evaluated with different duration times and departure dates, selecting eight possible solutions. All the candidate solutions respect the imposed constraints and not exceed the maximum fuel mass available for the spacecraft (250 kg),considering also a 20 % of margin. The solutions differ from duration time, $\Delta$V and stay time on the intermediate asteroids. At the beginning of the analysis a stay time of two months was considered for each asteroids, but in some solutions the optimal stay times are greater and it means more time for scientific research. Results shows also that increasing the duration mission is possible to obtain lower $\Delta$V, and,for equal durations, the departure date from Earth, and the arrive time on the intermediate asteroids are fundamental in propellant savings.

Possibles future works could be:

- once obtained the Ariel departure date and its orbital parameters, evaluate the escape from the lagrangian point L2, analyse the optimal trajectory and decide the optimal duration considering the mission costs;
- analyse and design the trajectories in proximity of the asteroids, evaluating strategies to stay in a stable orbit with the minimum propellant cost.

| Solution | $\Delta V$ [km/s] | Final Mass [kg] | Fuel Consumption [kg] | Duration (days) |
|---|---|---|---|---|
| 1A | 8.962 | 644 | 206 | 1395 |
| 1B | 8.341 | 657 | 193 | 1744 |
| 1C | 8.462 | 654 | 196 | 1395 |
| 1D | 8.333 | 657 | 193 | 1744 |
| 2A | 8.311 | 657 | 193 | 1569 |
| 2B | 8.193 | 660 | 190 | 1744 |
| 2C | 8.346 | 657 | 193 | 1569 |
| 2D | 7.959 | 665 | 185 | 1744 |

Table 6.1: Solutions Overview

It's important to remember that the asteroids selection process was based on known asteroids, and in the next future there could be an exponential growth of NEA discoveries. Some of the new asteroids could replace the chosen ones ,because more interesting in scientific terms or more convenient to reach. This could be made thanks to the electric propulsion flexibility which doesn't have limited launch windows , like chemical propulsion.

# Bibliography


[1] Nasa, Jet Propulsion Laboratory, Asteroids.

[2] Nasa, Jet Propulsion Laboratory, The Torino impact hazard scale.

[3] Nasa, Jet Propulsion Laboratory, The Palermo technical impact hazard scale.

[4] D.Farnocchia, S.R. Chesley, D.Vokrouhlicky,A. Milani, F. Spoto, W.F. Bottke, "Near Earth Asteroids with measurable Yarkovsky effect", Icarus 224 (2013)1-13.

[5] D.Farnocchia, S.R. Chesley, P.W. Chodas, M. Micheli, D.J. Tholen,,A. Milani, G.T. Elliot, F. Bernardi, "Yarkovsky-driven impact risk analysis for asteroid (99942) Apophis", Icarus 224 (2013), 192-200.

[6] M.Micheli, D.J. Tholen, G.T. Elliot, "2012 LA, an optimal astrometric target for radiation pressure detection", Icarus 226 (2013) 251-255.

[7] D.Vokrouhlicky, D.Farnocchia, D.Capek, S.R. Chesley, P. Pravec, P. Scheirich, T.G. Muller, "The Yarkovsky effect for 99942 Apophis", Icarus 252 (2015) 277-283.

[8] Roger R. Bate, Donald D. Mueller, Jerry E. White, "Fundamentals of Astrodynamics", Dover Publications, 1971.

[9] J.W. Cornelisse, H.F.R. Schöer, K.F.Wakker, "Rocket propulsion and spaceflight dynamics", Pitman, 1979.

[10] Robert G. Jahn, "Physics of Electric Propulsion", Dover Publications,1968.

[11] George P. Sutton, Oscar Biblarz, "Rocket Propulsion Elements", Jon Wiley & Sons, 2017.

[12] Lorenzo Casalino, Matthew A. Vavrina. ”Optimal power partitioning for electric thrusters”, AAS/AIAA Astrodynamics Specialist Conference, 2018.

[13] A.E. Bryson, Y.C. Ho, ”Applied Optimal Control”,Taylor & Francis Group, 1975.

[14] Lorenzo Casalino, ”Ottimizzazione Indiretta di traiettorie spaziali”.

[15] Lorenzo Casalino, ”Equazioni in coordinate sferiche”.

[16] Diffusion along mean motion resonance in the restricted planar three-body problem Contents - Scientific Figure on ResearchGate. Available from: https://www.researchgate.net/figure/Kirkwood-gapsfig

[17] CDF Study Report, SPP NEO inactive Body, ESA

[18] https://en.wikipedia.org/wiki/Near Earth object

[19] SURVEY OF TECHNOLOGIES RELEVANT TO DEFENSE FROM NEAR-EARTH OBJECTS - Scientific Figure on ResearchGate. Available from: https://www.researchgate.net/figure/Illustration-of-the-various-category-of-threat-under-the-Torino-Scale-fig10-24330508

[20] https://public.nrao.edu/gallery/yarkovsky-effect/

# Ringraziamenti

Vorrei ringraziare il professor Lorenzo Casalino per avermi guidato in questo percorso, per essere stato sempre disponibile a condividere le sue conoscenze fornendomi chiarimenti e consigli.

Un immenso grazie a Mamma e Papà, per avermi supportato (e sopportato) in questi lunghi anni; senza di voi non ce l'avrei mai fatta a raggiungere questo importante traguardo.

Un sincero grazie ai miei amici e compagni di corso, in particolare a Corrado, Luca, Marco G., Dario e Marco R.